JOURNAL OF GEOPHYSICAL RESEARCH, VOL. 96, NO. D5, PAGES 9075–9096, MAY 20, 1991

The Simplified Exchange Method Revisited: An Accurate, Rapid Method for Computation of Infrared Cooling Rates and Fluxes

M. DANIEL SCHWARZKOPF AND STEPHEN B. FELS[1]

NOAA Geophysical Fluid Dynamics Laboratory, Princeton University, New Jersey

The performance and construction of a new algorithm for the calculation of infrared cooling rates and fluxes in terrestrial general circulation models are described in detail. The computational method, which is suitable for use in models of both the troposphere and the middle atmosphere, incorporates effects now known to be important, such as an extended water vapor *e*-type continuum, careful treatment of water vapor lines, of water–carbon dioxide overlap, and of Voigt line shape. The competing requirements of accuracy and speed are both satisfied by extensive use of a generalization of the simplified exchange approximation of Fels and Schwarzkopf (1975). Cooling rates and fluxes are validated by comparison with benchmark line-by-line calculations on standard atmospheric profiles obtained for the Intercomparison of Radiation Codes Used in Climate Models (ICRCCM). Results indicate that the new algorithm is substantially more accurate than any previously used at the Geophysical Fluid Dynamics Laboratory.

1. INTRODUCTION

The construction of a radiation code for use in general circulation models involves a balance between conflicting considerations of speed and accuracy. The requirement for speed may be formulated, in general terms, as a demand that the time spent in computing radiative cooling rates and fluxes be reasonably short with respect to the computation time of the rest of the model. This condition forces the use of highly parameterized, approximate approaches in the radiative computations. The requirement for accuracy is less simple to quantify, but clearly radiation codes should reflect up-to-date understanding of the important contributors to the determination of cooling rates and fluxes. Systematic errors in the radiative algorithm can lead to errors in general circulation model climatologies, which, while unimportant for short range forecasts, have serious effects in longer range predictions and in climate studies.

The conflict between speed and accuracy is particularly acute in the calculation of longwave radiative cooling rates and fluxes, the subject of this paper. Usually, the computation of infrared radiative quantities in general circulation models takes far longer than the corresponding shortwave calculations. The reasons for this are rather complex, and the situation may well change as more complete calculations of scattering are incorporated in numerical models, but they primarily are caused by two factors: first, longwave radiation has sources at every level of the atmosphere, while shortwave radiation has only one source; second, longwave radiation depends strongly on atmospheric temperature, while shortwave radiation is, to good accuracy, independent of temperature.

In an attempt to resolve these difficulties, *Fels and Schwarzkopf* [1975] (hereinafter referred to as FS75) introduced the simplified exchange approximation (SEA), a method which produces accurate and rapid computations of infrared cooling rates and fluxes, particularly those resulting from water vapor line absorption. Subsequently, the authors formulated methods for calculating carbon dioxide cooling rates and fluxes by interpolation from precomputed CO_2 transmissivities [*Fels and Schwarzkopf*, 1981 (FS81); *Schwarzkopf and Fels*, 1985 (SF85)]. Using the techniques discussed in the above papers, a computer program calculating longwave cooling rates and fluxes was written for inclusion in general circulation models at the Geophysical Fluid Dynamics Laboratory (GFDL). This program is now in use in several operational numerical models both at GFDL and elsewhere. The performance of these operational radiation codes is discussed by *Fels et al.* [this issue].

Since the development of this procedure, several advances in the field of longwave radiative transfer have taken place, which suggest the need for a major reconsideration of the above methods. New experimental data for line strengths, widths, and positions are readily available, due to publication of revisions to the Air Force Geophysics Laboratory (AFGL) catalog of lines in the infrared spectrum [*McClatchey et al.*, 1973; *Rothman*, 1981; *Rothman et al.*, 1983, 1987]. A comparable atlas of lines has also been developed by *Chedin et al.* [1985]. The AFGL catalog now gives reliable values for line positions for the gaseous absorbers of interest in the thermal infrared. The values for line strengths and widths are less certain, especially for the highly excited "hot" bands of the molecules, but are obtained from a variety of recent laboratory measurements. Most important, the catalogs are sufficiently comprehensive (and computers sufficiently powerful) to permit detailed radiative computations employing these data. It is now possible to compute fluxes by brute-force summation of absorptivities from all lines in the catalog at all required frequency points. This method, known as the line-by-line (LBL) technique, is free of many assumptions made in other computational methods, and thus may be expected to provide more exact values for longwave cooling rates and fluxes than those previously available.

Progress has also been made in recent years in evaluating

[1]Deceased October 22, 1989.

Paper number 89JD01598.

the observed excess absorption due to H_2O at wavelengths far from the water vapor rotation or vibration-rotation band. This excess, usually denoted as H_2O continuum absorption, has been ascribed to a number of causes, including H_2O dimer effects [e.g., *Suck et al.*, 1979] and distant wings of water vapor absorption lines [e.g., *Clough et al.*, 1980]. No attempt was made in FS75 to include this absorption, which depends on the partial pressure of water vapor (and thus on the square of the H_2O mixing ratio). A number of experimental measurements of this absorption have now been made (cf. *Grant* [1987] for a review of these measurements). Continuum absorption is now believed to vitally affect the calculated cooling rates and fluxes in the 400–1200 cm^{-1} frequency region.

An important stimulus for improvement in calculations of longwave radiative transfer has been the WMO-sponsored Intercomparison of Radiation Codes in Climate Models (ICRCCM). A general description of ICRCCM, and of initial clear-sky longwave results is contained in the work by *Luther et al.* [1988]. In brief, the ICRCCM study consists of computations by various methods of longwave and shortwave cooling rates and fluxes, for both clear-sky and cloudy cases, on standard temperature and absorber profiles. In the context of this paper, we consider only the longwave clear-sky results, which are the most complete. The longwave cases employ five standard AFGL temperature, water vapor, and ozone profiles (given by *McClatchey et al.* [1971]). These are denoted as the tropical (T), mid-latitude summer (MLS), mid-latitude winter (MLW), sub-Arctic summer (SAS), and sub-Arctic winter (SAW). Individual ICRCCM cases may include one or more gaseous absorbers (including the H_2O continuum), as well as a CO_2 amount of either 300 or 600 ppmv. The computational methods used range from LBL methods to the highly parameterized methods used in general circulation models.

A major result of ICRCCM has been the establishment of benchmark values for cooling rates and fluxes for the standard profiles mentioned above. To achieve this goal, line-by-line computations were performed for a number of ICRCCM cases by up to three different groups. Each group used somewhat different assumptions for line shapes of the gaseous absorbers. Line data were taken from the two catalogs mentioned above. Upon intercomparison, these computations were seen to obtain essentially the same cooling rates and fluxes [*Luther et al.*, 1988; *World Meteorological Organization* (WMO), 1984; *Ridgway et al.*, this issue]. This agreement has given researchers considerable confidence that these LBL computations may be considered "exact," given the spectral input data. Benchmark LBL fluxes and cooling rates have now been tabulated for a large number of cases employing the standard profiles.

Comparison of LBL results with corresponding results obtained using approximate models has permitted reevaluation of the less detailed calculations. In the first place, a number of computer code errors have been discovered in various schemes (including the GFDL code based on FS75). More important, it is now possible to calibrate the highly parameterized schemes used in operational models by comparison of their results for standard cases to the LBL values. Operational radiation codes calibrated in this manner should be far more accurate than those employing previous methods, such as tuning to a random model (as in FS75) or to broad-band measurements of absorption. For instance, LBL methods do not need scaling approximations to treat temperature and pressure variations over optical paths, such as are required by random models. Also, the line data used for the LBL calculations are directly applicable to atmospheric concentrations, temperatures and pressures of interest, whereas broad-band measurements, especially for water vapor, are generally taken at conditions not found in actual terrestrial atmospheres.

Benchmark calculations have been used to gain insight into a number of problems removed from the calibration of operational models. For example, *Ramanathan and Downey* [1986*a*] have shown that the use of wide bands in random models leads to large errors in upper tropospheric cooling rates as compared to the LBL results. LBL calculations have been used to determine the most accurate methods for handling H_2O-CO_2 overlap in the 15 μm frequency region [*Schwarzkopf*, 1986]. An important and continuing use of LBL calculations is in determining the accuracy of scaling approximations, particularly for ozone, for which current methods are inaccurate [*Rodgers*, 1968].

All of these developments have taken place in parallel with spectacular advances in computer power occurring since the radiation codes used at GFDL were written. As a result, operational radiation codes are now expected to include more sophisticated calculations of the effects of longwave radiation; in addition, these codes are being used in general circulation models that possess increased horizontal and vertical resolution, and which may, in certain applications, compute longwave cooling rates at short time intervals. It thus is vital that any revised radiation algorithm possess sufficient speed to permit unrestricted use in future operational models.

In subsequent sections of this paper, we outline a method which, we believe, meets the tests of both increased accuracy and adequate speed. Section 2 is an overview of the approach, including differences and similarities to the methods of FS75. In section 3, we discuss the accuracy of the new method by showing overall results for five standard ICRCCM soundings. The results from this section represent the heart of this paper. The reader who is not concerned with details of the model may skip sections 4 and 5, which provide details of model construction and model performance in the troposphere and stratosphere, respectively. Section 6 is a brief discussion of the vital question of the model speed. The concluding section consists of a summary and cautionary note.

2. Overview of the Method

In the absence of scattering, the clear-sky radiative cooling rate Q at pressure p is readily obtained from monochromatic transmissivities, using the following expressions:

$$Q(p) = c_p^{-1} g \frac{d}{dp} \int_0^\infty F_\nu(p)\, d\nu \tag{1}$$

$$F_\nu(p) = B_\nu[T(0)]\tau_\nu(0, p) + \int_0^{p'} \frac{\partial B_\nu}{\partial p'} \tau_\nu(p, p')\, dp' \tag{2}$$

TABLE 1. Primary and Secondary Absorbing Mechanisms in Infrared Frequency Ranges

	Frequency Range, cm^{-1}						
	0–400	400–560	560–800	800–990	990–1070	1070–1200	1200–2200
Primary absorbers	H_2O (L)	H_2O (L)	H_2O (L) H_2O (C) CO_2	H_2O (C)	H_2O (C) O_3	H_2O (C)	H_2O (L)
Secondary absorbers		H_2O (C)	O_3	H_2O (L)	H_2O (L) CO_2	O_3	

All secondary mechanisms are included only in the random CTS calculation. H_2O lines are denoted H_2O (L), and the H_2O continuum is denoted H_2O (C).

$$\tau_\nu(p, p') = 2\int_0^1 \mu\, d\mu \prod^{\text{gases}} \cdot \exp\left\{\frac{-1}{\mu g}\int_p^{p'} r^{\text{gas}}(p'')\sum_k f_k^{\text{gas}}(\nu, T(p''), p'')\, dp''\right\} \quad (3)$$

In the above relations, c_p is the specific heat of dry air at constant pressure, g is the gravitation constant, $F_\nu(p)$ the net radiative flux at frequency ν and pressure p, B_ν the blackbody function at frequency ν, τ_ν the monochromatic transmission function including all absorbers between pressure levels p and p', p^s the surface pressure, μ the cosine of the zenith angle, r^{gas} the mass mixing ratio for a gaseous absorber, and f_k^{gas} the absorption coefficient at frequency ν due to the kth spectral line of a gaseous absorber.

Cooling rates obtained using (1)–(3) are denoted as LBL cooling rates. The line strengths and line widths used to determine absorption coefficients are taken from the 1982 AFGL line catalog [*Rothman et al.*, 1983]. The 1986 AFGL catalog was unavailable when the calculations for most of this study were made; use of the newer catalog is not expected to significantly alter the results.

In practical computations, the LBL method is far too time-consuming to permit its use in operational numerical models. The reason is that absorption lines in the infrared spectrum are typically about 0.1 cm^{-1} in width at a standard pressure (1 atm). At low pressures, the lines become sufficiently narrow that absorptivities change significantly over frequency intervals of as small as 10^{-3} cm^{-1}. Since the frequency integration in (1) must be evaluated over the entire infrared spectrum, a range of about 2000 cm^{-1}, and numerous absorption lines are found throughout this range, about 10^6 frequency points are required to produce a LBL calculation of high accuracy. The time spent in such calculations is so substantial, even on current computers, that the LBL method is usable, in practice, only for selected benchmark calculations.

A number of approximations to the LBL method have been developed which allow the replacement of the monochromatic calculations with averages over intervals of between 5 and 10 cm^{-1} (narrow-band random models), the use of homogeneous paths to replace the inhomogeneous paths encountered in the atmosphere (scaling methods), and the use of a diffusivity factor to replace the integration over zenith angle. The resulting parameterizations have been shown to suffer little loss of accuracy relative to LBL calculations [*Ramanathan and Downey*, 1986*a*; *Crisp et al.*, 1986]. Although these methods are far more rapid than the LBL method, they still are too time consuming for use in most large-scale numerical models. First, they still require a relatively large number (50–100) of frequency bands. Also, in many of these frequency bands (such as around the 15 μm region) the calculations are rather complex, often involving absorption arising from several physically distinct mechanisms.

Further increases in the speed of the radiative calculations would result if two additional approximations were made: neglecting less important absorption processes at a particular frequency interval, and ignoring some of the complexities of the narrow-band random model calculations to allow the use of wider frequency bands. In a given frequency interval, there usually will be a primary absorption mechanism which dominates over others. In Table 1, we decompose the infrared spectrum extending from 0 to 2200 cm^{-1} into a series of frequency ranges, indicating in each the primary and secondary absorption mechanisms. The neglect of the secondary mechanisms, and the use of approximate methods allowing an entire frequency range to be computed as one band, would reduce the number of required frequency intervals to as few as five to ten. Of course, calculations using these approximations are less accurate than the narrow-band computations; clearly, we desire a method which incorporates the increased speed obtained by these approximations, yet retains the accuracy of the narrow-band methods.

One method for achieving this goal of rapid, accurate radiative calculations is the SEA, first introduced in FS75. The SEA recognizes that, in many circumstances, the dominant contribution to cooling rates at a given height comes from the "cool-to-space" (CTS) term [*Rodgers and Walshaw*, 1966]. The cool-to-space cooling rate (Q_{CTS}) is relatively easy to compute, since it requires only the transmission function between the level in question and space, as opposed to the full calculation, which requires the transmission between this level and all other levels:

$$Q_{\text{CTS}} = c_p^{-1} g \int_0^\infty B_\nu(T)\frac{\partial \tau(0, p)}{\partial p}\, d\nu \quad (4)$$

By definition, the contribution to the cooling rate Q that is not included in the CTS term is called the exchange term, and one can therefore define

$$Q = Q_{\text{ex}} + Q_{\text{CTS}} \quad (5)$$

The basic premise of the SEA is that the cooling rates due to the exchange term may be calculated using approximate techniques, with little loss of accuracy:

$$Q_{ex} \approx Q_{ex}^{app} \tag{6}$$

and therefore

$$Q \approx Q_{ex}^{app} + Q_{CTS} \tag{7}$$

Since the cooling rate (Q^{app}) obtained using the approximate techniques also is the sum of the exchange and CTS terms, (7) may be written

$$Q \approx Q^{app} - Q_{CTS}^{app} + Q_{CTS} \tag{8}$$

As it stands, (8) is still not suitable for practical computations, since Q_{CTS} is (by definition) an LBL calculation. We have already indicated, however, that narrow-band random approximations to Q_{CTS} are available which incorporate virtually all of the relevant physical mechanisms and, in addition, are relatively fast. Thus the operational version of the SEA, to be used in the rest of this paper, is

$$Q \approx Q^{app} - Q_{CTS}^{app} + Q_{CTS}^{random} \tag{9}$$

All of the terms in (9) may be computed easily and rapidly. In the case of the first two terms (Q_{ex}^{app}) this is due to the use of highly simplified physics, which allows the calculations to be performed on a few very wide frequency bands. The random CTS term is obtained using methods developed in section 4; in this case, although a larger number of relatively narrow frequency bands must be used, the simplicity of the calculation in each frequency interval permits rapid evaluation. As a result, the SEA provides a compromise approach providing both sufficient speed and accuracy for operational numerical model calculations.

Before turning to a discussion of the techniques used to obtain Q_{ex}^{app}, we present an example which demonstrates the accuracy of the SEA hypothesis (6). We do so by comparing a LBL calculation of the cooling rate terms of (5) to a similar computation using (7), with Q^{app} and Q_{ex}^{app} obtained using an extremely rapid, approximate method to be described subsequently. The principal results are displayed in Figures 1*a* and 1*b*. We observe that in the troposphere neither Q^{app} nor Q_{CTS} is close to Q(LBL); however, the SEA hypothesis is very successful. It is useful to note that Q_{ex} is small compared to Q(LBL) for all pressures greater than ~0.1 mbar. Above this level, Q_{ex} is an important contributor to Q(LBL), in general agreement with *Leovy* [1984].

The original form of the SEA (described in detail in FS75 and denoted here as SEA75) consisted simply of the use of an emissivity calculation for Q_{ex}^{app} in those parts of the spectrum for which water vapor lines are the primary absorbing mechanism. In this paper, we describe a generalization of the SEA (denoted as SEA88) which permits application of the SEA to all frequency ranges in the infrared spectrum. The exchange term in SEA88 is an approximate calculation for the primary absorption mechanism in each of the frequency ranges given in Table 1. The random CTS term includes both the primary and the less important (secondary) mechanisms. Since this term is computed on relatively narrow frequency bands, it may also be used to correct for errors caused by the use of wide frequency bands in the approximate calculations.

It is important to realize that the composition of the approximations used for the exchange term in SEA88 can vary from spectral interval to spectral interval. Similarly, the additional effects included in the random CTS term will differ in each frequency range. In general, these effects are of three types: (1) incorporation of complexities in the radiative calculations, (2) correction of errors caused by the use of wide frequency intervals in the approximate calculations, and (3) inclusion of the secondary absorption mechanisms given in Table 1. For example, in frequency ranges in which water vapor lines are the sole primary absorber, the approximate technique employed is an emissivity calculation (dis-

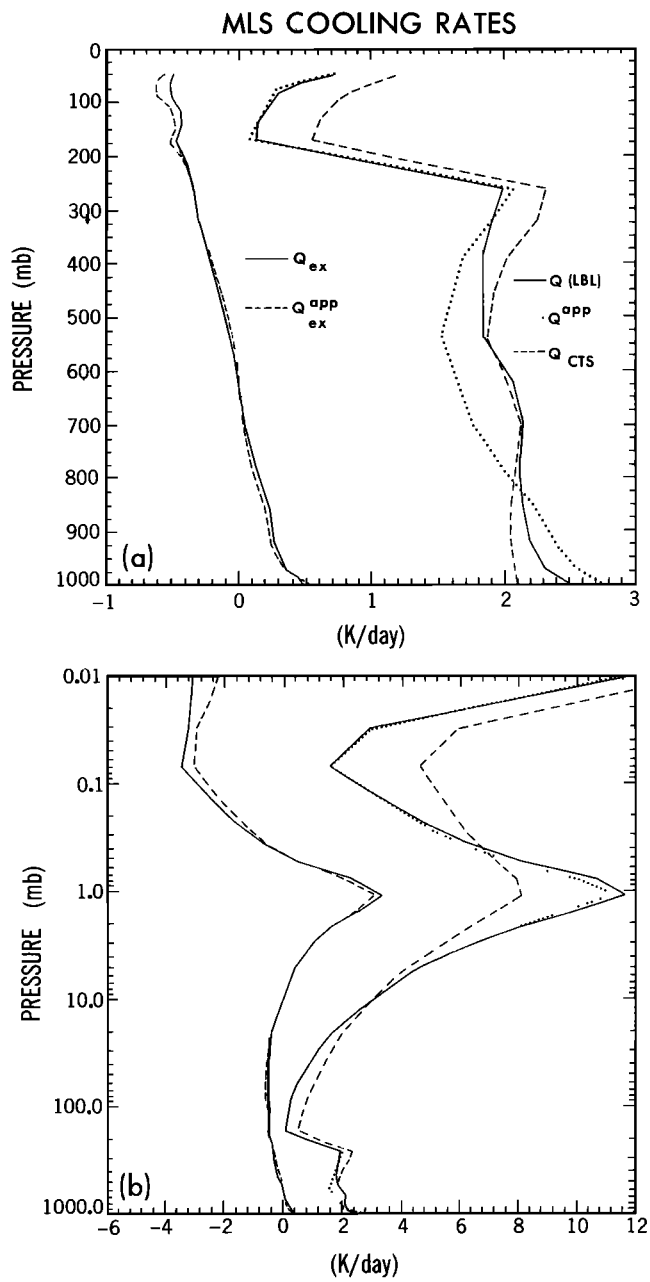

Fig. 1. Cooling rates (in K/d) for the AFGL mid-latitude summer (MLS) profile with the absorbers H_2O, CO_2, O_3, and the water vapor continuum included. The three curves on the right side of the figure give the line-by-line cooling rate (Q(LBL)), the LBL cool-to-space cooling rate (Q_{CTS}), and Q^{app}, obtained by the methods given in this paper. The two curves on the left side of the figure give Q_{ex} (defined in (6)) and Q_{ex}^{app}. In Figure 1*a*, tropospheric results are emphasized, with the ordinate being pressure, ranging from 0 to 1000 mbar. In Figure 1*b*, middle atmosphere results are emphasized; the ordinate is pressure, ranging from 1000 to 0.01 mbar on a logarithmic scale.

cussed in detail in section 4). As shown in FS75, the use of an emissivity approximation for transmissivities leads to enormous efficiencies, but degraded accuracy. The random CTS term here is used primarily to incorporate effects due to the variation of H_2O line strength with temperature. In the frequency range including the 15-μm region (560–800 cm^{-1}), where absorption by carbon dioxide, water vapor lines, and continuum are all significant, the exchange term is computed using one frequency interval, thus treating crudely the overlap of the gaseous absorbers. The random CTS term uses two frequency intervals to account for the frequency dependence of the overlap (see section 4 for further details). Finally, in the portion of the spectrum where absorption by the water vapor continuum dominates, the exchange term is a wide-band computation including only the absorption due to the continuum, while the random CTS term includes the effects of water vapor lines, as well as the variation of the continuum coefficient with frequency.

As the above discussion suggests, application of SEA88 in each frequency range involves considerable computational detail. We postpone such details to sections 4 and 5 in order to first display overall results for benchmark cases over the entire longwave spectrum.

3. Overall Results

As discussed in section 1, the existence of benchmark values for longwave cooling rates and fluxes now permits rigorous checking of any parameterized method, at least in the absence of clouds. We therefore have computed cooling rates and fluxes for the five standard ICRCCM profiles using the radiation algorithm given in this paper. These cooling rates (denoted henceforth as SEA88) are displayed in Figures 2*a*–6*b*, together with cooling rates for the same profiles obtained using LBL methods. Also shown are cooling rates computed using the operational radiation code based on FS75 (denoted as SEA75). For each calculation we show two figures, one emphasizing the troposphere and one the stratosphere and mesosphere (middle atmosphere). The appendix provides details of the methods for obtaining pressure, temperature, water vapor and ozone profiles from the AFGL data. The pressure level structures used in the LBL and operational model calculations are also described in this appendix.

Tropospheric cooling rates for the five standard cases are displayed in Figures 2*a*–6*a*. In all five cases, at nearly all pressures, cooling rates obtained using the new radiation algorithm (SEA88) are substantially closer to the LBL values than those obtained using SEA75. Errors in cooling rates computed using SEA88 are generally 0.1 K/d. The most noticeable differences (up to 0.2 K/d) occur in the 250- to 350-mbar pressure range. Much of this difference is artificial, resulting from comparing LBL calculations using high (20 mbar) vertical resolution at these pressures with calculations of the operational models (with ~70-mbar vertical resolution). To eliminate this effect, we have obtained "degraded" LBL cooling rates for the operational model pressure levels, using techniques outlined in the appendix. Figure 7*a* displays the differences between the operational model results and the "degraded" LBL values for the MLS profile; for pressures greater than 200 mbar, the SEA88 calculations give errors below 0.1 K/d and are far superior to the SEA75 results. Details on the computational methods used to obtain the SEA88 results will be given in section 4.

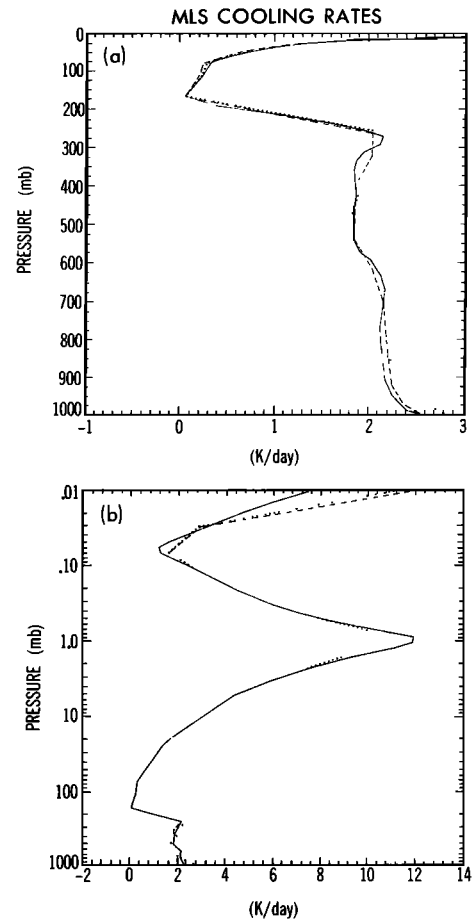

Fig. 2. Cooling rates (in K/d) for the AFGL mid-latitude summer (MLS) profile with the absorbers H_2O, CO_2, O_3, and the water vapor continuum included. Cooling rates are evaluated over the 0–2200 cm^{-1} frequency range. The solid line gives cooling rates obtained using LBL methods, the dashed line gives results obtained using the new (SEA88) radiation algorithm, and the dotted line gives results obtained using the SEA75 radiation algorithm. As in Figure 1, two figures are presented, with tropospheric results in Figure 2*a* and middle atmosphere results in Figure 2*b*.

The excellent agreement in tropospheric cooling rates suggests that fluxes obtained using the new method should also agree closely with fluxes obtained using LBL methods. We have computed the net fluxes at the top of the atmosphere, the tropopause and the ground for the five ICRCCM cases, and display results in Table 2. As expected, results from SEA88 agree much more closely with the LBL results than those from SEA75.

Middle atmosphere cooling rates for the same five cases are shown in Figures 2*b*–6*b*. As in the troposphere, cooling rates computed using the new radiation algorithm are generally in excellent agreement with the LBL results. In this case, the agreement is less surprising, since both SEA88 and SEA75 obtain CO_2 cooling rates using the methods given in FS81 and SF85. Again, some of the discrepancies between the LBL and operational model results are caused by resolution effects, and may be eliminated by use of degraded LBL cooling rates. Differences between the operational model cooling rates and the degraded LBL results for the MLS profile are shown in Figure 7*b*; the largest values occur near 1 mbar, amounting to ~0.9 K/d. Section 5 provides

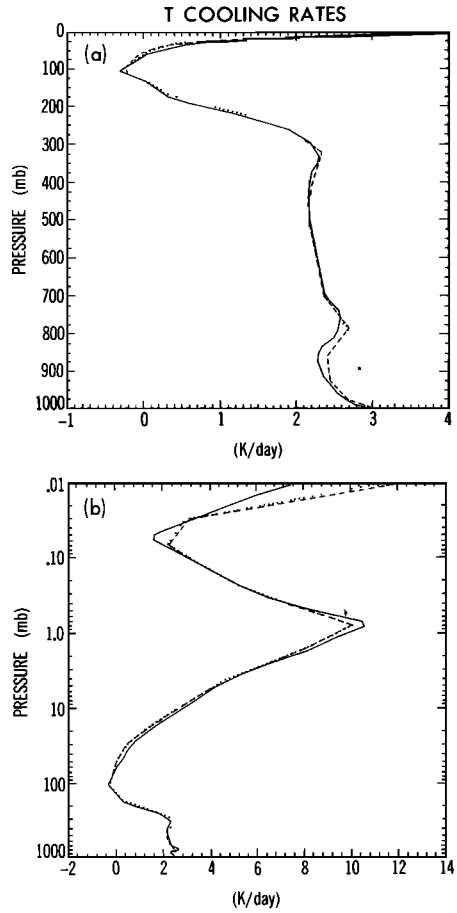

Fig. 3. Same as Figure 2, but with cooling rates for the AFGL tropical (T) profile.

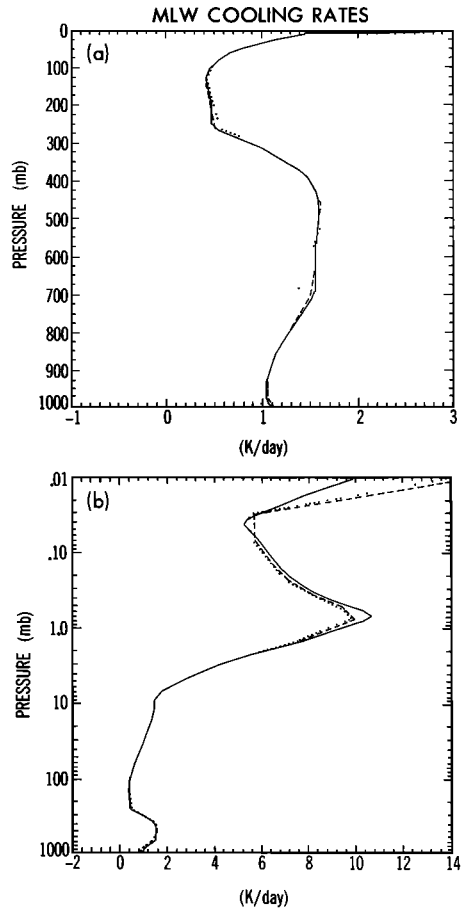

Fig. 4. Same as Figure 2, but with cooling rates for the AFGL mid-latitude winter (MLW) profile.

further discussion of these differences, and of the small but important errors noticeable in the lower stratosphere.

4. Tropospheric Issues and Computational Methods

Water vapor absorption is the most important contributor to tropospheric infrared cooling rates. As noted in Table 1, absorption due to either water vapor lines or the *e*-type H_2O continuum is significant at all frequencies in the thermal infrared. Our main focus, in this section, is on cooling rates due to water vapor only. The inclusion of CO_2 cooling rates is discussed in a subsection on 15 μm band cooling rates; radiative effects of ozone, significant only in the middle atmosphere, are discussed in section 5.

We begin by displaying cooling rates due to water vapor (including the *e*-type H_2O continuum) for the MLS and T soundings (Figures 8*a* and 9*a*), and due to water vapor (lines only) for the MLS profile (Figure 10*a*). In order to avoid resolution effects, degraded LBL cooling rates are employed for all comparisons between LBL and parameterized calculations in this section. The operational model results are for the old (SEA75) and new (SEA88) radiation algorithms. Differences between the operational model cooling rates and the LBL results are shown in Figures 8*b*–10*b*. As in the computations with all gases, cooling rates computed using SEA88 are substantially more accurate (i.e., closer to the LBL results) than those obtained using SEA75. The only pressure region where the SEA88 algorithm does not improve the results is between 900 and 1000 mbar, in the lines-only comparison (Figure 10*b*). Possible reasons for errors in that region will be discussed below.

We next break down the tropospheric water vapor cooling rates into values for various frequency domains. As noted in Table 1, the infrared spectrum may be divided into several frequency ranges, each with differing radiative properties. In the 0–560 and 1200–2200 cm^{-1} ranges, water vapor is the only significant absorbing mechanism. The 800–1200 cm^{-1} range has the H_2O continuum as the principal absorbing mechanism, with the H_2O lines and ozone playing a secondary role. In the 560–800 cm^{-1} region, both H_2O (lines and continuum) and CO_2 are important absorbing mechanisms. The contribution from each frequency range to cooling rates varies with altitude. We show this in Figure 11, where LBL cooling rates for the water vapor lines-only case using the MLS sounding are shown as a function of pressure for various frequency ranges. Two points to notice are (1) cooling between 200 and 300 mbar is overwhelmingly the result of absorption in the spectral range between 160 and 560 cm^{-1}, and (2) most cooling near the surface is due to lines in the 560–800 cm^{-1} region. Figure 12 is the corresponding picture for LBL calculations with only the water vapor continuum included, while Figure 13 displays results for the LBL calculation including H_2O lines and continuum. The principal difference between these results and those of

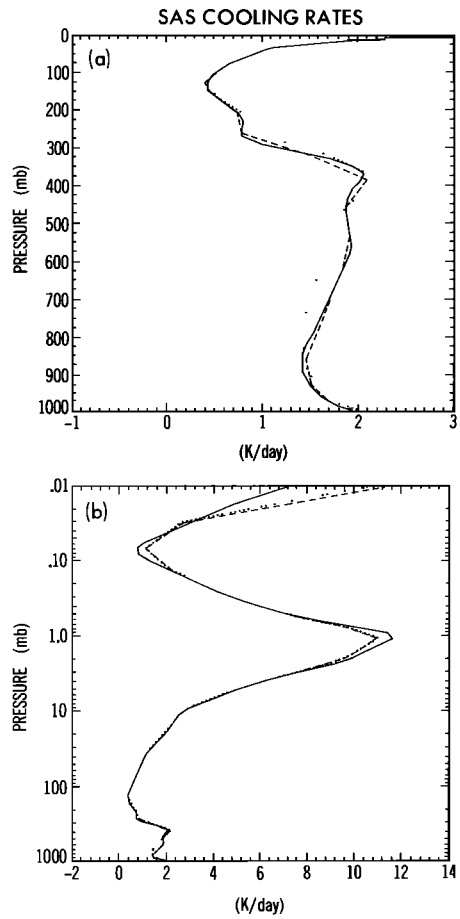

Fig. 5. Same as Figure 2, but with cooling rates for the AFGL sub-Arctic summer (SAS) profile.

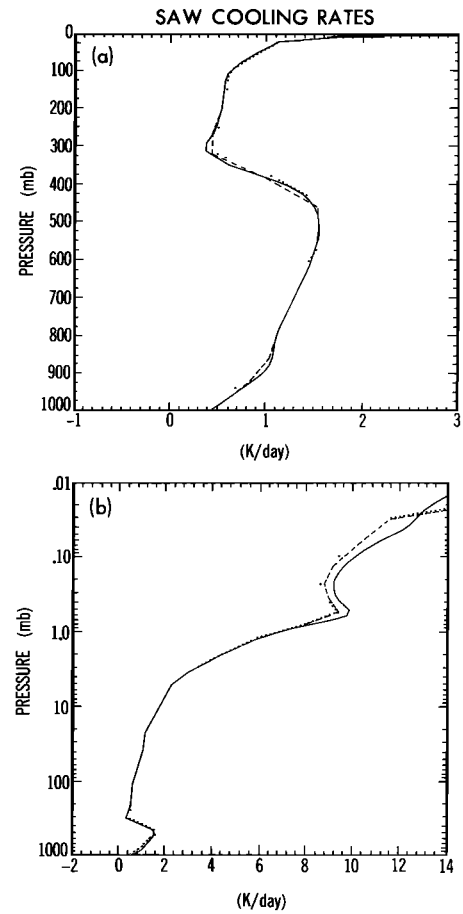

Fig. 6. Same as Figure 2, but with cooling rates for the AFGL sub-Arctic winter (SAW) profile.

the lines-only case is in the 800–1200 cm^{-1} range near the surface, where cooling due to the continuum dominates. Increased cooling between 800 and 900 mbar is due to continuum absorption in the 560–800 cm^{-1} range; the effect of the continuum between 400 and 560 cm^{-1} is an increase in cooling between 600 and 700 mbar, and a reduction near the surface.

In the subsections below, we describe the methods used to obtain the SEA88 results in each frequency range, using the LBL results of Figures 11–13 for purposes of validation.

Water Vapor Lines-Only Region

Absorption due to water vapor lines is the principal mechanism contributing to cooling rates in the 0–560 and 1200–2200 cm^{-1} frequency ranges. We therefore may apply (9) in these frequency regions by taking Q^{app} to be simplified calculation of H_2O cooling rates. In SEA88, just as in SEA75, we have employed an emissivity calculation applied to a Goody random model.

The emissivity approximation ignores the variation of line intensity with temperature along the path between two pressures. Further, it assumes that the strong-line approximation may be used to compute transmissivities. In the strong-line approximation, the transmission function for an inhomogeneous path depends only on the pressure-scaled absorber amount $U(p, p')$:

$$U(p, p') = p_0^{-1} \int_p^{p'} p'' \, du \tag{10}$$

The standard pressure p_0 = 1013.25 mbar; u is the absorber amount. If the variation of line intensity with temperature is also ignored, the flux at pressure p can be shown to depend on the emissivity $G(T, U)$:

$$G(T, U) = T^{-4} \int_0^{\infty} B_\nu(T) \tau^{sl}(T_0, U) \, d\nu \tag{11}$$

In (11), τ^{sl} is the transmissivity computed using the strong-line approximation at a standard temperature T_0 (250 K).

To apply the emissivity approximation in random models, we write

$$G(T, U) = T^{-4} \sum_n B_n(T) \tau_n(U, T_0) \Delta\nu_n \tag{12}$$

with

$$\tau_n(U, T_0) = \exp\left[-(\alpha_n(T_0) DU(p, p'))^{1/2}\right] \tag{13}$$

and

$$\alpha_n(T_0) = \frac{2}{\Delta\nu_n} \sum_k \left[S_k(T_0) \gamma_k(T_0, p_0)\right]^{1/2} \tag{14}$$

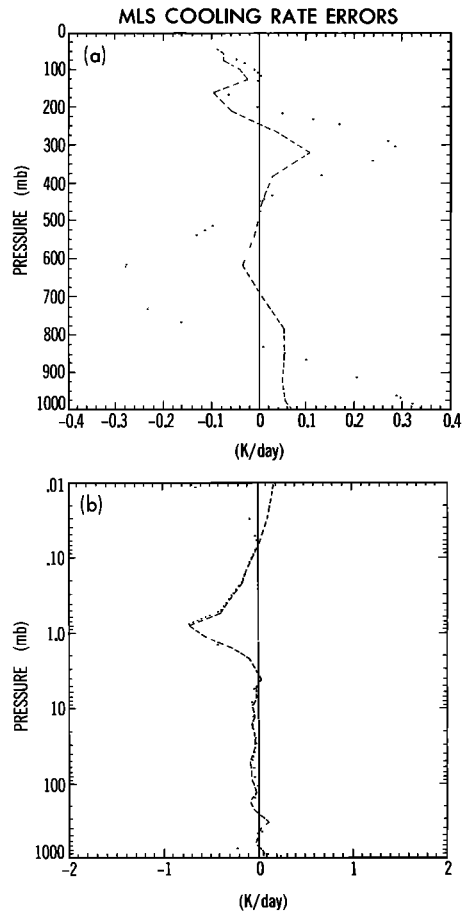

Fig. 7. Cooling rate errors (in K/d) for the AFGL MLS profile. The dashed line gives the difference in cooling rate between the SEA88 computation and the LBL calculation (i.e., Q(SEA88) − Q(LBL)). The LBL values are degraded to the resolution used for the SEA88 calculations. The dotted line gives the difference in cooling rate between the SEA75 computation and the LBL calculation. Figure 7*a* emphasizes the errors in the troposphere, while Figure 7*b* emphasizes the middle atmosphere errors.

In (14), S_k and γ_k are line intensities and widths at the standard temperature (T_0) and pressure (p_0) for line k in frequency interval n, and the sum is over all lines in the frequency interval. $\Delta\nu_n$ is the bandwidth for the frequency interval. $B_n(T)$ is the blackbody function integrated over the frequency interval at temperature T. The values of S_k and γ_k are derived from laboratory data on line widths and strengths contained in the 1982 version of the AFGL catalog [*Rothman et al.*, 1983]. In (13), D is the diffusivity factor, specified as 1.66 for all water vapor calculations. The flux at pressure level p computed using the emissivity approximation may then be written as

$$F(p) = G_1[T(0), U(0, p)]T^4(0) + \int_0^{p^s} \frac{\partial T^4}{\partial p'} G_2[T(p'), U(p', p)]\, dp' \qquad (15)$$

with

$$G_1(T, U) = T^{-4} \sum_n B_n(T)\tau_n(T_0, U)\Delta\nu_n \qquad (16)$$

and

$$G_2(T, U) = \tfrac{1}{4} T^{-3} \sum_n \frac{\partial B_n(T)}{\partial T} \tau_n(T_0, U)\Delta\nu_n \qquad (17)$$

The great advantage of employing the emissivity approximation is that the functions $G_1(T, U)$ and $G_2(T, U)$ in (16) and (17) can be precomputed, thus making the computation extremely efficient. The frequency range for the summations in (16) and (17) is the entire water vapor lines-only region (0–560, 1200–2200 cm^{-1}). This range differs from that of SEA75, in which (by implication) the entire longwave spectrum was included.

The random CTS cooling rate at pressure p is evaluated using the following expression:

$$Q_{\text{CTS}}^{\text{random}} = c_p^{-1} g \sum_n B_n(T) \frac{\partial \tau_n(0, p)}{\partial p} \Delta\nu_n \qquad (18)$$

In this case, $\tau_n(0, p)$ is obtained using the Goody random model. Temperature scaling [see *Rodgers and Walshaw*, 1966] is employed to account for the variation of line properties with temperature, with T_0 = 250 K and line strengths computed at 25 K intervals. The 1982 AFGL catalog is used for line data. The important issue of the specification of frequency bands used in computing the random CTS term is discussed below.

Approximate CTS cooling rates are obtained by evaluating (18) with the transmission function $\tau_n(0, p)$ computed by using the emissivity approximation (13) and (14). As in the computation for Q^{app}, this calculation may be performed using the precalculated emissivity function $G_1(T, U)$, with $T = T(p)$ and $U = U(0, p)$.

The chief problem for radiative computations in this frequency region is the selection of frequency bands over which to evaluate Q^{app} and $Q_{\text{CTS}}^{\text{random}}$. In SEA75, the precomputed emissivities as well as the random CTS terms were evaluated over the frequency bands proposed by *Rodgers and Walshaw* [1966]. These bands are about 100 cm^{-1} wide; six bands are used in the 0–560 cm^{-1} region, while eight are employed in the 1200–2200 cm^{-1} region. Recently, however, *Ramanathan and Downey* [1986*a*] have shown that cooling rates in the upper troposphere computed using broad-band random models have substantial errors (up to 0.5 K/d) when compared with LBL results. Best agreement with LBL computations is attained with band widths of no more than 10 cm^{-1}. This finding is directly applicable to calculations using the emissivity approximation; we show this by displaying, in Figure 14, the difference between LBL cooling rates for the MLS profile and cooling rates obtained using two emissivity calculations: one employs 10 cm^{-1} bands for the entire frequency domain (0–560, 1200–2200 cm^{-1}), while the other uses 100 cm^{-1} bands in the 160–560 cm^{-1} region and 10 cm^{-1} bands elsewhere. In the 250- to 350-mbar region the 100 cm^{-1} calculation overestimates cooling by about 0.2 K/d, whereas the 10 cm^{-1} calculation is much more accurate, as in Ramanathan and Downey. Both emissivity computations underestimate cooling rates in the middle troposphere by about 0.15 K/d, showing that in this region the most important issue is the variation of line intensity with temperature, as discussed in FS75, rather than the width of the spectral bands.

The foregoing results lead naturally to a specification of

TABLE 2. Net Longwave Fluxes (in W/m^2) at the Top of the Atmosphere, Tropopause, and Surface for the Five ICRCCM Cases

Model	Case				
	T	MLS	MLW	SAS	SAW
			Net Surface Flux		
LBL	66.49	79.07	91.89	90.24	82.91
OLD	58.87	76.25	95.98	90.04	81.80
NEW	64.22	77.06	94.09	88.46	82.71
(OLD − LBL)	−7.62	−2.82	4.09	−0.20	−1.11
(NEW − LBL)	−2.27	−2.01	2.20	−1.78	−0.20
			Net Tropopause Flux		
LBL	288.11	272.77	214.57	239.25	178.21
OLD	286.66	270.86	211.94	236.93	175.64
NEW	288.18	272.55	213.89	238.98	177.48
(OLD − LBL)	−1.45	−1.91	−2.63	−2.32	−2.57
(NEW − LBL)	0.07	−0.22	−0.68	−0.27	−0.73
			Upward Flux at Top		
LBL	298.28	288.99	236.56	269.96	202.95
OLD	295.77	286.53	234.34	268.00	201.40
NEW	296.91	287.79	235.51	268.84	202.35
(OLD − LBL)	−2.51	−2.46	−2.22	−1.96	−1.55
(NEW − LBL)	−1.37	−1.20	−1.05	−1.12	−0.60

The tropical case is denoted as T, the mid-latitude summer case as MLS, the mid-latitude winter case as MLW, the sub-Arctic summer case as SAS, and the sub-Arctic winter case as SAW. Models used are the line-by-line (LBL), the old operational model (OLD), and the new algorithm (NEW). Tropopause pressures are 93.7 mbar (T case), 179.0 mbar (MLS case), 256.8 mbar (MLW case), 267.5 mbar (SAS case), and 282.9 mbar (SAW case). The LBL calculations are made on a 0–2200 cm^{-1} frequency range with the 1982 AFGL catalog used for line data.

Q^{app} as the cooling rate computed using the emissivity approximation evaluated on 10 cm^{-1} wide bands, and Q_{CTS}^{random} as the cool-to-space water vapor cooling rate, computed on the same 10 cm^{-1} wide bands. Figure 15 displays the differences between cooling rates for the 0–560 and 1200–2200 cm^{-1} region obtained with this SEA specification and with the LBL method; also shown are the errors arising from the use of Q^{app} alone. The SEA substantially reduces cooling rate errors at nearly all pressures; the only noticeable errors are in the 600- to 700-mbar region, where cooling rates are underestimated by ~0.08 K/d.

The problem with this calculation is that far too many bands are required in the random CTS computation, thus making the method unacceptably slow. We have been able to reduce the number of bands required to a number suitable for practical computations by employing a number of strategems. First, we assume that the CTS correction to Q^{app} is unimportant in the 0–160 and 1200–2200 cm^{-1} regions. To justify this approximation, we note that the temperature dependence of water vapor lines of frequencies greater than 1000 cm^{-1} is known to be small [*Rodgers and Walshaw*, 1966]. The emissivity approximation should thus be sufficiently accurate at these frequencies. In addition, LBL cooling rates in the 0–160 and 1200–2200 cm^{-1} region are small (cf. Figure 11), both in magnitude and in proportion to cooling rates from other frequency domains. In any case, examination of Figures 11 and 13 indicates that the error due to this approximation is acceptably small.

No such approximation is possible in the 160–560 cm^{-1} region, which includes the strongest water vapor lines in the infrared spectrum. In this region, the H_2O transmissivity varies enormously with frequency, even when the transmissivity is expressed as an average over a 10 cm^{-1} interval. If we assume that the transmission function in this region is given by the strong-line approximation of the Goody random model, we may obtain the coefficient α_n (defined in (14)). Figure 16 is a plot of α_n in each 10 cm^{-1} interval. We see that α_n takes on a wide range of values; however, it is also evident that similar values for α_n are obtained in several frequency intervals. We exploit this fact by consolidating 10 cm^{-1} bands with similar values for α_n into a smaller number of "combined narrow" bands, and using these combined bands in the random CTS calculations. To accomplish this, we first obtain random model parameters for a combined narrow band (N) using the laboratory data contained in the AFGL catalog. Next, the transmissivity $\tau_N(0, p)$ for band N is obtained using the above random parameters. The random CTS cooling rate for band N is computed by using the following expression:

$$Q_{CTS}^{random}(N) = c_p^{-1} g \frac{\partial \tau_n(0, p)}{\partial p} \sum_{n'} B_{n'}(T) \qquad (19)$$

where the sum over n' is over all of the 10 cm^{-1} bands comprising the combined narrow band (N). (It is important to note that the values of $\Sigma B_{n'}(T)$ are obtained by table lookup of precomputed blackbody functions evaluated over specified frequency ranges at specified temperatures; therefore no additional computation time is necessary to obtain the values of the source function required by any combined narrow band.) The final step is the summation of these cooling rates over all combined narrow bands to obtain the random CTS cooling rates for the frequency range. The specification of the combined narrow bands is shown in Table 3. Eight such bands are employed for the 160–560 cm^{-1} range, with four of these bands in the 160–400 cm^{-1} frequency range and four other bands between 400 and 560 cm^{-1}.

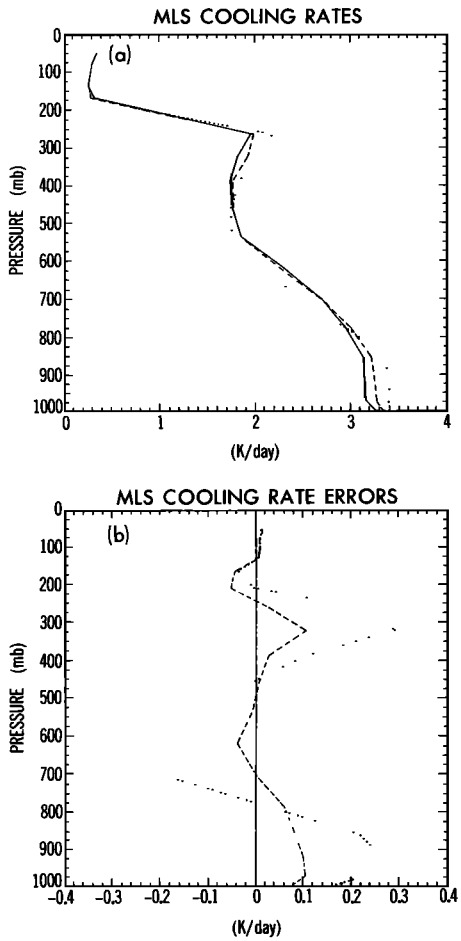

Fig. 8. (*a*) Cooling rates for the MLS profile. Absorption from H_2O (lines plus continuum) is included. The solid line gives degraded LBL results, the dashed line gives results for SEA88, and the dotted line gives results for SEA75. (*b*) Cooling rate errors for the MLS profile, with absorption from H_2O (lines plus continuum) included. The dashed line gives errors due to the SEA88 computation, and the dotted line errors owing to the SEA75 formulation, as in Figure 7*a*. Tropospheric results are emphasized.

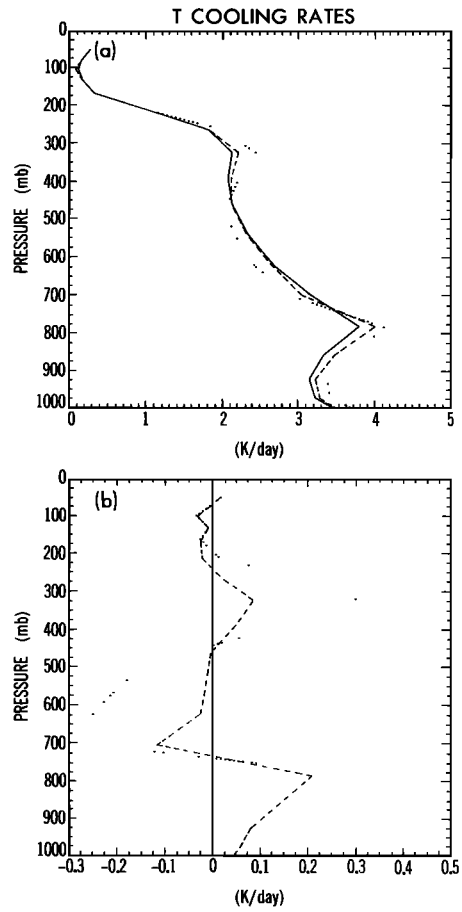

Fig. 9. (*a*) Same as Figure 8, but with cooling rates for the T profile. (*b*) Same as Figure 8*b*, but with cooling rate errors for the T profile.

The effect of using combined narrow bands in SEA88 is shown in Figure 17, where errors due to this approach are compared with those arising when 10 cm^{-1} wide bands are used. We see that the combined narrow band approximation (with eight bands in the 160–560 cm^{-1} range) yields cooling rates for the MLS profile which are remarkably close to the more elaborate method (with 40 bands in that range).

In creating these combined narrow bands, a deliberate effort was made to separate bands with frequencies greater than 400 cm^{-1} from those of smaller frequencies. Above 400 cm^{-1}, water vapor absorption in excess of that attributable to lines is observed, and denoted as H_2O continuum absorption. The LBL calculations displayed in Figures 11–13 indicate that this mechanism should be significant between 700 mbar and the surface. We include this absorption in the random CTS computation, using the same expressions that are used for the 10-μm region, discussed below. This approach is consistent with the overall philosophy of inclusion of secondary effects in the random CTS calculations. In Figure 18 we show the error in the SEA88 calculation made by including this effect in the random CTS term, as well as the error resulting from entirely neglecting the continuum absorption. It is evident that the SEA88 computation is able to account for most of the extra absorption.

The 10-μm Region

We next turn to the frequency region between 800 and 1200 cm^{-1}. For the present, we ignore the presence of absorbers other than water vapor. Inspection of Figures 11 and 13 indicates that this region differs from the lines-only region in two respects: first, most absorption is attributable to the water vapor continuum; second, most cooling takes place near the surface. We therefor apply the SEA in this region by defining Q^{app} as a one-band computation of cooling rates due only to the H_2O continuum. Water vapor lines, as well as the variation of the continuum coefficient with frequency, are included as secondary effects in the random CTS calculation.

The major difficulty in computing H_2O continuum cooling rates arises from the dependence of the absorption coefficient on the partial pressure of water vapor rather than on the mean atmospheric pressure over the path. In general, we may write the continuum transmission function as

$$\tau_\nu(p, p') = \exp\,[-k_\nu(T)Du] \tag{20}$$

with

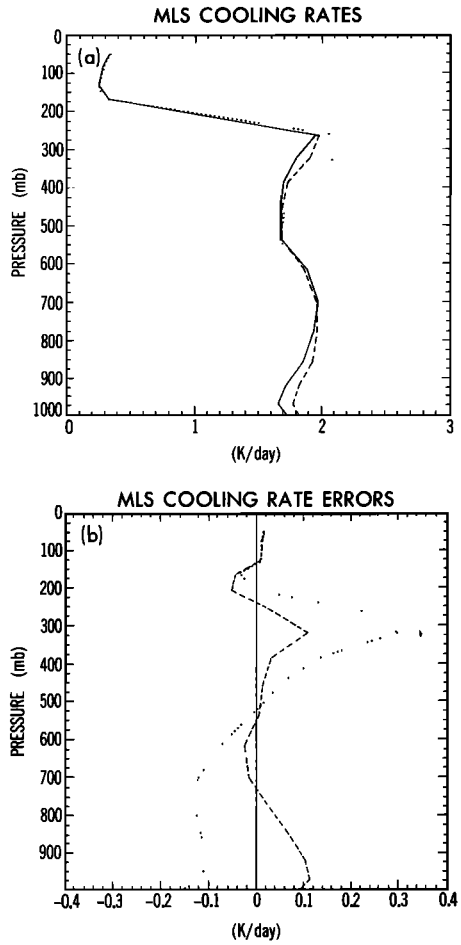

Fig. 10. (*a*) Same as Figure 8*a*, but absorption from H_2O (lines only) is included. (*b*) Same as Figure 8*b*, but absorption from H_2O (lines only) is included.

$$k_\nu(T) = \alpha_\nu(T)e(H_2O) + \beta_\nu(T)p \tag{21}$$

In (20) and (21), e is the partial pressure of H_2O, u the H_2O amount between pressures p and p', and α_ν and β_ν the continuum coefficients for e-type and p-type absorptions, respectively. D in (20) is the diffusivity factor, which is taken as 1.66. Were $k_\nu(T)$ only a function of pressure, the effect of the continuum could easily be incorporated in an emissivity calculation, since $\tau(p, p')$ would depend only on temperature and the pressure-scaled mass. One would merely extend the frequency range used in precomputing emissivities, incorporating continuum transmissivities obtained using (20) in appropriate frequency ranges. The actual dependence of $k_\nu(T)$ on $e(H_2O)$ (and thus on the square of the H_2O mixing ratio) forces us to treat this frequency range separately.

In the present formulation (SEA88), we assume that $\beta_\nu(T) = 0$, and that $\alpha_\nu(T)$ is obtained as in *Roberts* [1976]. To obtain one-band continuum coefficients for Q^{app}, we merely compute

$$k(\Delta\nu) = \frac{1}{\Delta\nu}\int_{\nu_2}^{\nu_1} k_\nu(296)\, d\nu \tag{22}$$

over the frequency interval ($\nu_1 = 800\ cm^{-1}$, $\nu_2 = 1200\ cm^{-1}$) at 296 K.

The random CTS computation is designed to include water vapor lines (using the Goody random model) and to allow for the variation of continuum coefficient with frequency. (The variation of $\alpha_\nu(T)$ with temperature is frequency independent; we have chosen to include this effect in both the Q^{app} and the random CTS calculations.) Since the continuum coefficient actually changes gradually with frequency, and the inclusion of water vapor lines in this frequency range affects cooling rates only in the surface region (cf. Figures 12 and 13), we may use wider frequency bands in this region

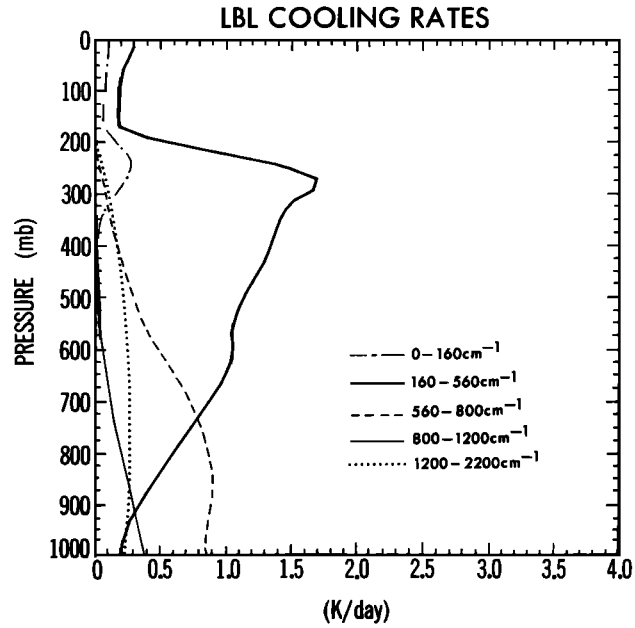

Fig. 11. Cooling rates by frequency range for the MLS profile using the LBL method. The absorber is H_2O (lines only). The frequency ranges included are 0–160, 160–560, 560–800, 800–1200, and 1200–2200 cm^{-1}.

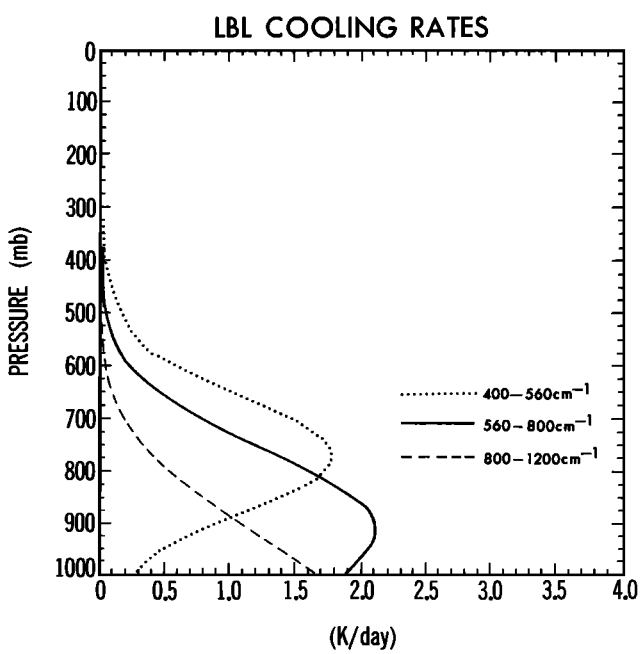

Fig. 12. Same as Figure 11, but the absorber is H_2O (continuum), and the frequency ranges included are 400–560, 560–800, and 800–1200 cm^{-1}.

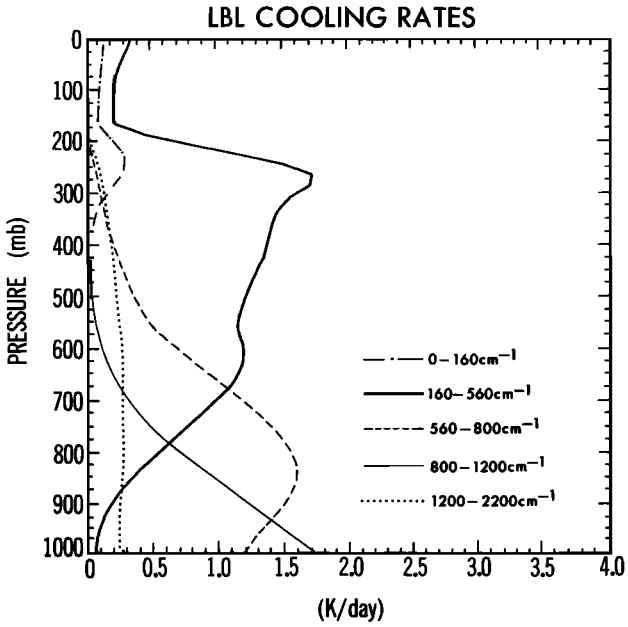

Fig. 13. Same as Figure 11, but the absorber is H_2O (lines plus continuum).

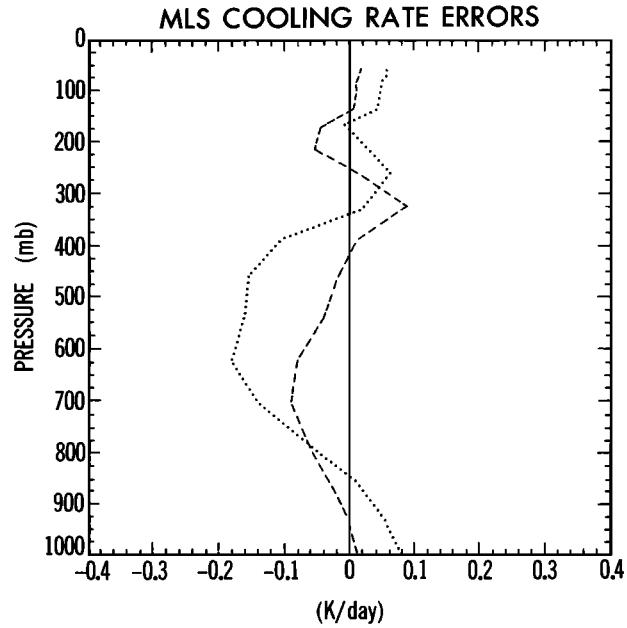

Fig. 15. Same as Figure 14, but the dotted line gives errors using the emissivity calculation with 10 cm^{-1} bandwidth in the 160–560 cm^{-1} frequency range, and the dashed line gives errors using the SEA formulation, with a 10 cm^{-1} bandwidth used for calculation of the random CTS term.

than in the lines-only region. In SEA88, we have employed four frequency bands in the random CTS calculation. The frequency range of these bands is given in Table 3.

We now compare the SEA88 results with the LBL values in this frequency range. Figure 19 displays the differences in the continuum-only case; plotted are errors made by SEA88,

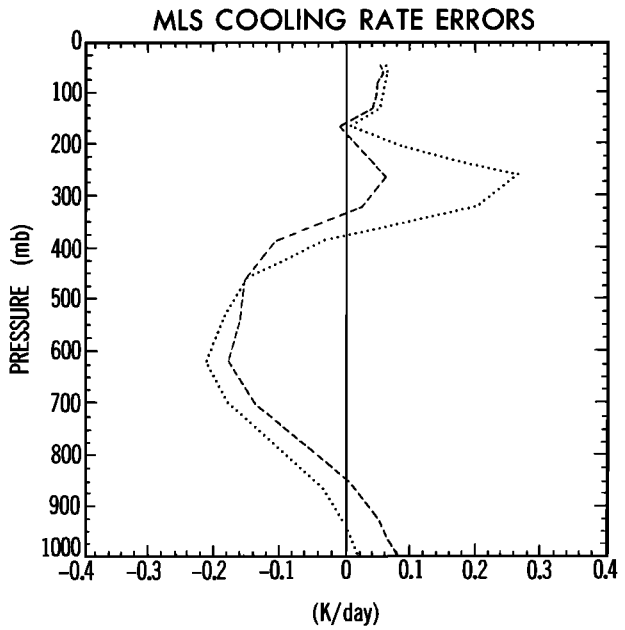

Fig. 14. Cooling rate errors for the MLS profile in the H_2O (lines only) case. The frequency range used is 0–560 and 1200–2200 cm^{-1}. The dashed line gives errors owing to an emissivity calculation with 10 cm^{-1} bandwidth in the 160–560 cm^{-1} range, while the dotted line gives errors using an emissivity calculation with 100 cm^{-1} bandwidth in the 160–560 cm^{-1} range. Both calculations use the same bandwidth in the rest of the frequency range. Differences are given as $Q - Q$(LBL), as in Figure 7*a*. The LBL cooling rates are shown in Figure 11.

as well as those made using only Q^{app}. Figure 20 shows the corresponding results with the water vapor lines now included. In each case, errors using the SEA88 formulation are less than 0.1 K/d at all pressures, while the approximate calculation (which does not include water vapor lines) gives errors of as much as 0.35 K/d.

In practice, some modifications to the parameterization described above are required, owing to the existence of the strong absorption band of ozone at 9.6 μm. As indicated in Table 1, ozone is an important contributor (in the middle atmosphere) to cooling rates in the 990–1070 cm^{-1} interval. In SEA88 we have excluded this frequency region from the 10-μm frequency range. The one-band computation Q^{app} is therefore performed on a single band comprising the 800–990 and 1070–1200 cm^{-1} range. The 990–1070 cm^{-1} frequency interval is computed as a separate frequency range. Results in the 990–1070 cm^{-1} range, with ozone included, will be discussed in section 5.

The 15-μm Region

The 560–800 cm^{-1} frequency range differs from the lines-only and 10-μm region in that we must now include three significant contributors to tropospheric cooling rates: H_2O lines, H_2O continuum, and CO_2. Our approach here is to calculate Q^{app} over one frequency band which comprises the entire frequency interval, using simple calculations for each of the absorbers. The random CTS calculation includes a more complete calculation of H_2O line absorption, and attempts to correct for the error committed in a one-band treatment of CO_2-H_2O overlap.

Transmission functions Q^{app} are computed separately for each gas over the 560–800 cm^{-1} interval, and multiplied to obtain the combined transmissivity used in cooling rate computations. For CO_2, a computer code initially formu-

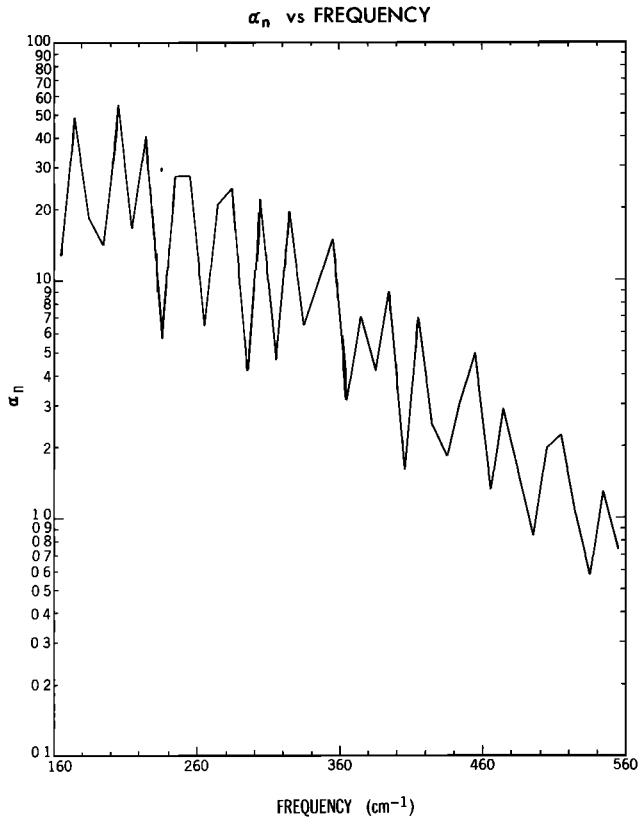

Fig. 16. Absorption by H_2O as a function of frequency. For each 10 cm^{-1} band between 160 and 560 cm^{-1}, the absorption coefficient α_n (defined in (14)) is evaluated. The ordinate gives values of α_n, and the abscissa gives frequencies (in cm^{-1}). In the new operational model, frequency bands with similar values of α_n are grouped to form the combined narrow bands listed in Table 3.

lated by *Drayson* [1973] has been used to obtain LBL transmission functions for a standard temperature profile. The methods given in FS81 and SF85 are then used to obtain transmissivities appropriate for the particular temperature and pressure profile. The H_2O continuum is included in a manner similar to the one-band calculation for the 10-μm band, with the continuum coefficient averaged over the 560–800 cm^{-1} interval using (22). Transmissivities for H_2O lines are obtained using the emissivity approximation (12) and (13), with all band parameters evaluated at 250 K. We assume that errors due to the neglect of variation of band parameters with temperature will be corrected by inclusion of these effects in the random CTS calculation.

The principal function of the random CTS calculation is to account for errors resulting from the use of only one band in the Q^{app} calculation, which results in an overly crude treatment of H_2O-CO_2 overlap. In general, band models obtain the transmission function in frequency intervals containing more than one gaseous absorber by multiplication of the band transmissivities computed for each absorber. In the 15-μm region, this procedure is as follows:

$$\tau_{\Delta\nu}(p, p') = \tau_{\Delta\nu}(H_2O)\tau_{\Delta\nu}(CO_2)\tau_{\Delta\nu}(\text{cont}) \quad (23)$$

In this relation, $\Delta\nu$ is the bandwidth. By contrast, LBL calculations in this region are done as follows:

$$\tau_{\nu}(p, p') = \tau_{\nu}(H_2O)\tau_{\nu}(CO_2)\tau_{\nu}(\text{cont}) \quad (24)$$

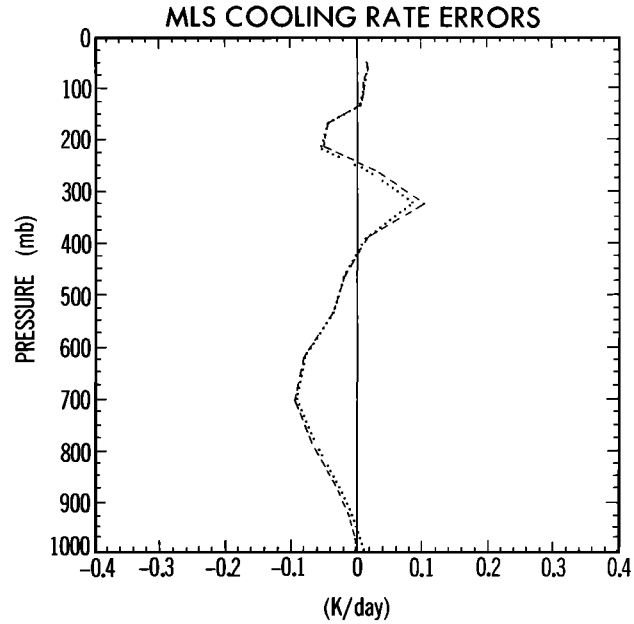

Fig. 17. Same as Figure 14, but the dotted line gives errors for the SEA calculation using 10 cm^{-1} bands for the random CTS term, while the dashed line gives errors for the SEA88 algorithm described in (19) and related text.

$$\tau_{\Delta\nu}(p, p') = \frac{1}{\Delta\nu}\int_{\nu_2}^{\nu_1} \tau_{\nu}(p, p')\, d\nu \quad (25)$$

For each method, cooling rates and fluxes for the frequency interval may be obtained through use of (2) and (1). Cooling rates for the entire 15-μm band are then obtained by summation over the number of frequency intervals.

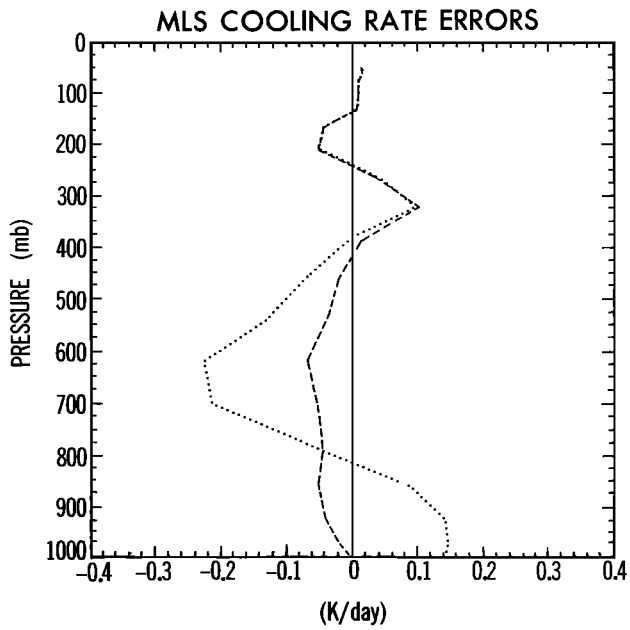

Fig. 18. Cooling rate errors for the MLS profile due to the H_2O continuum in the 400–560 cm^{-1} frequency range. The dotted line gives errors when the continuum absorption is neglected; the dashed line gives errors using the SEA88 formulation, with the H_2O continuum included. The LBL cooling rates for H_2O (lines plus continuum) are given in Figure 13.

TABLE 3. Band Structure Used for the New Radiation Algorithm

Frequency Range, cm^{-1}	Approximate Calculation	Random CTS Calculation
0–160	Sum over 16 bands of 10 cm^{-1} width	
160–560	Sum over 40 bands of 10 cm^{-1} width	Eight bands: 1. 170–180, 200–210, 220–230 2. 160–170, 180–190, 190–200, 210–220, 240–250, 250–260, 270–280, 280–290, 300–310, 320–330, 350–360 3. 230–240, 260–270, 330–340, 340–350, 370–380, 390–400 4. 290–300, 310–320, 360–370, 380–390 5. 410–420, 450–460 6. 420–430, 440–450, 470–480, 500–510, 510–520 7. 400–410, 430–440, 460–470, 480–490 8. 490–500, 520–530, 530–540, 540–550, 550–560
560–800	One band, 240 cm^{-1} wide	Two bands 1. 560–670 2. 670–800
800–900	One band, including the 800–900, 900–990, and 1070–1200 cm^{-1} ranges	One band
900–990	See 800–900 cm^{-1} range	One band
990–1070	One band, 80 cm^{-1} wide	One band
1070–1200	See 800–900 cm^{-1} range	One band
1200–2200	Sum over 100 bands of 10 cm^{-1} width	

The bands given in the approximate calculation column are used in computing Q^{app}. The same bands are used in obtaining Q^{app}_{CTS}, but only the frequency ranges from 160 to 1200 cm^{-1} are used. Bands given in the random CTS calculation column are used for the random cool-to-space calculation.

In principle, significant differences may be expected between transmissivities obtained by the band model method (23) and by the LBL approach (25). For the same bandwidth, $\tau_{\Delta\nu}$ obtained using (23) will diverge from the same quantity computed using (25), particularly as the bandwidth increases. Eventually, this will result in unacceptable errors in cooling rates and fluxes in the 15-μm region.

Clearly we need to determine a bandwidth which is sufficiently narrow to permit accurate calculations of cooling rates and fluxes, yet wide enough that the random CTS calculations may be performed using a small number of frequency bands. To do so, we have used the LBL method

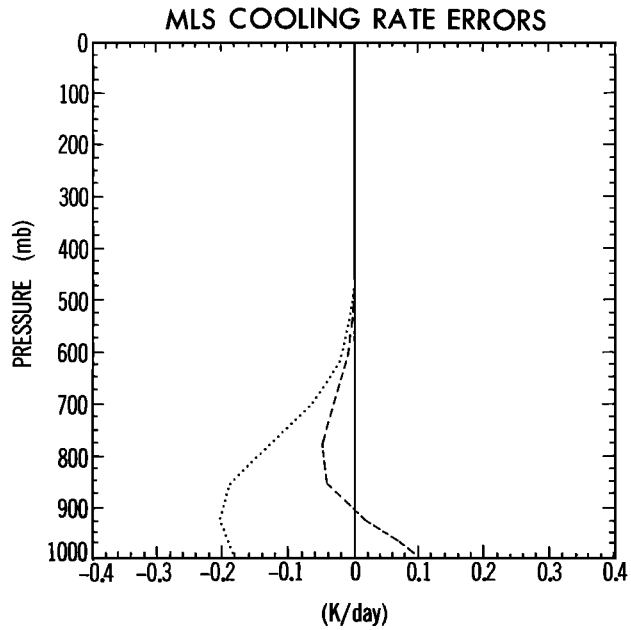

Fig. 19. Cooling rate errors for the MLS profile in the H_2O continuum-only case. The frequency range used is 800–1200 cm^{-1}. The dotted line is the one-band (Q^{app}) error, and the dashed line the error of the SEA88 formulation. The LBL cooling rates are given in Figure 12.

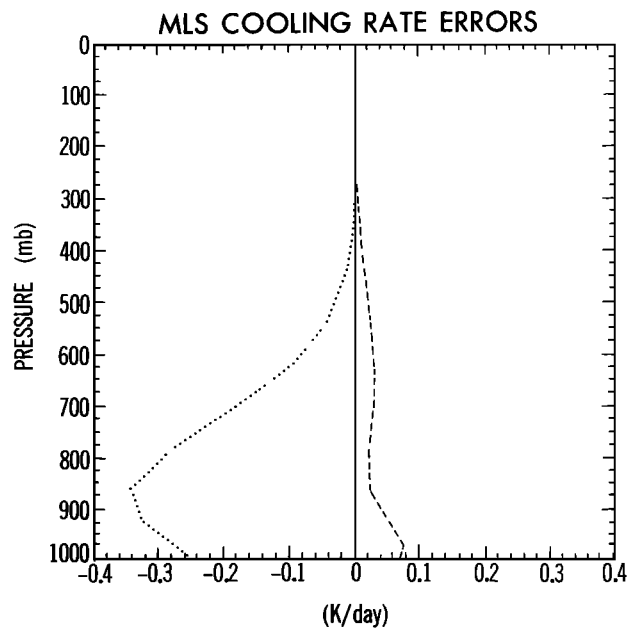

Fig. 20. Same as Figure 19 but for the H_2O (lines plus continuum) case. The LBL cooling rates are given in Figure 13.

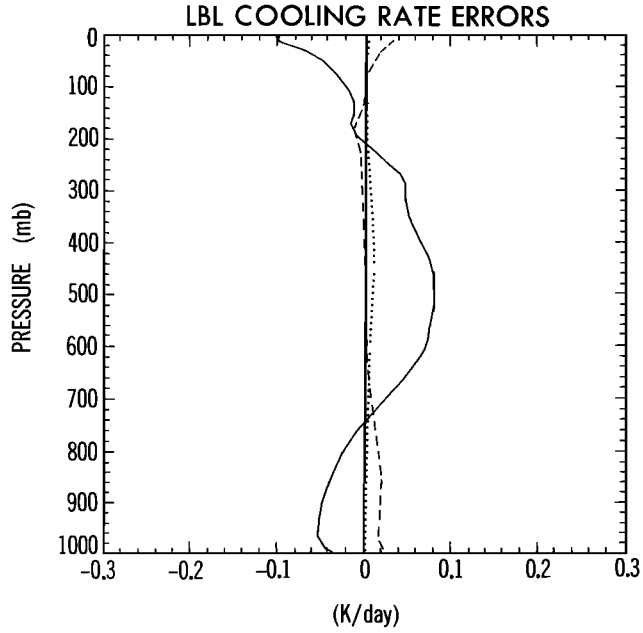

Fig. 21. Cooling rate errors due to the treatment of overlap in the 600–800 cm^{-1} range. The MLS profile is used, and the absorbers are CO_2 and H_2O (lines only). The dotted line gives the difference between the cooling rate computed with a 10 cm^{-1} bandwidth and the LBL result. The dashed line is the same quantity, with a 100 cm^{-1} bandwidth employed. The solid line is the same result with a 200 cm^{-1} bandwidth used.

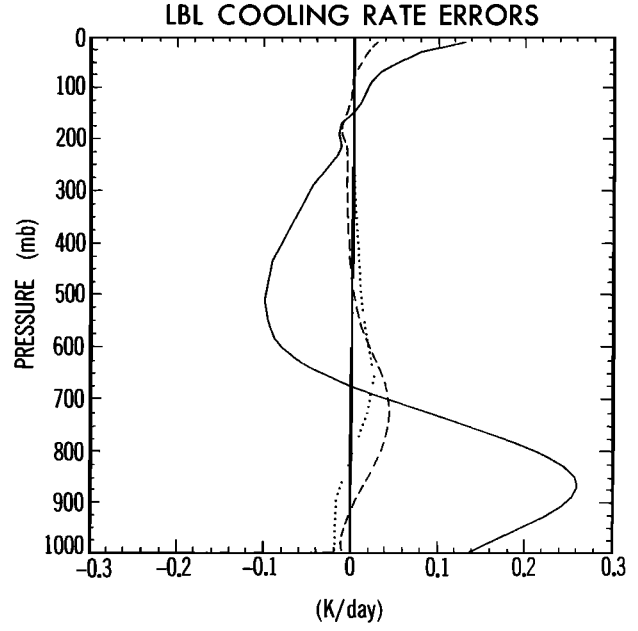

Fig. 22. Same as Figure 21 but the absorbers are CO_2 and H_2O (lines plus continuum).

to obtain $\tau_{\Delta\nu}(p, p')$ separately for H_2O, CO_2, and the continuum. Integration over a specified bandwidth, as in (25), yields band transmissivities for each absorber, obtained by the LBL technique, but otherwise comparable to the band transmissivities obtained using band models. Multiplication of these transmissivities, as in (23), produces a combined transmissivity $\tau_{\Delta\nu}(p, p')$ comparable to that obtained by the band model calculation. By using (1) and (2), we may obtain 15-μm band cooling rates for the specified bandwidth. Differences between these cooling rates and the benchmark LBL values may then be attributed to the bandwidth used for this calculation.

To determine the desired bandwidth, cooling rates have been computed for the 600–800 cm^{-1} interval, using the method outlined above, and compared to the LBL values. Five values of bandwidth were employed: 10, 20, 50, 100, and 200 cm^{-1}. These computations have been performed for two cases: (1) CO_2 + H_2O lines and (2) CO_2 + H_2O lines and continuum. The MLS profile was used for temperature and H_2O mixing ratio, and the CO_2 mixing ratio was 300 ppmv. Results for the two cases are shown in Figure 21 (CO_2 + H_2O lines) and Figure 22 (CO_2 + H_2O lines and continuum). In each figure we display error curves for the band model computations using bandwidths of 10, 100, and 200 cm^{-1}. It is surprising that when lines only are considered, bandwidths of 100 cm^{-1} give excellent results, and even a bandwidth of 200 cm^{-1} is acceptable. When the continuum is included, however, bandwidths of 100 cm^{-1} are required to retain accuracy. We conclude that two frequency bands with bandwidths of about 100 cm^{-1} are sufficient to account for H_2O-CO_2 overlap in the 15-μm region.

The above considerations have been used to formulate the SEA88 algorithm in the 15-μm region. First, we compute Q^{app} by using one-band transmissivities defined over the 560–800 cm^{-1} frequency range. The random CTS computations are then performed using two frequency intervals. In practice, the first band extends from 560 to 670 cm^{-1}, and the second from 670 to 800 cm^{-1}. In each band, H_2O transmissivities for both lines and continuum are obtained; the effects of temperature on line intensity are included. CO_2 transmission functions for each band are obtained from LBL transmissivities, using the methods of FS81 and SF85. Figure 23*a* displays the cooling rate errors made by this approach, together with the errors made using Q^{app}. The LBL cooling rates used for comparison are shown in Figure 23*b*. Considerable improvements in lower tropospheric heating rates are evident, a result which appears to justify the additional computational time spent in this region.

5. Middle Atmosphere Issues and Computational Methods

Infrared cooling in the middle atmosphere is primarily caused by absorption due to lines in the 15-μm band complex of CO_2 and in the 9.6-μm band of O_3. Absorption by water vapor lines also contributes significantly to cooling, especially in the 10- to 100-mbar region, but cooling rates due to H_2O are always smaller than that due to the other two absorbers. Contributions of other gases (CH_4, N_2O, etc.) are of minor importance and will not be considered in this paper.

The design of algorithms for the computation of middle atmospheric cooling rates in general circulation models raises a number of issues that do not arise in the tropospheric computations described in section 4. Radiative computations in the middle atmosphere differ from tropospheric computations in three important ways. First, ozone is an important contributor to middle atmospheric cooling rates, especially in the lower stratosphere and near the stratopause. Second, at low pressures, it becomes necessary to use the Voigt line shape rather than the Lorentz line shape to obtain accurate

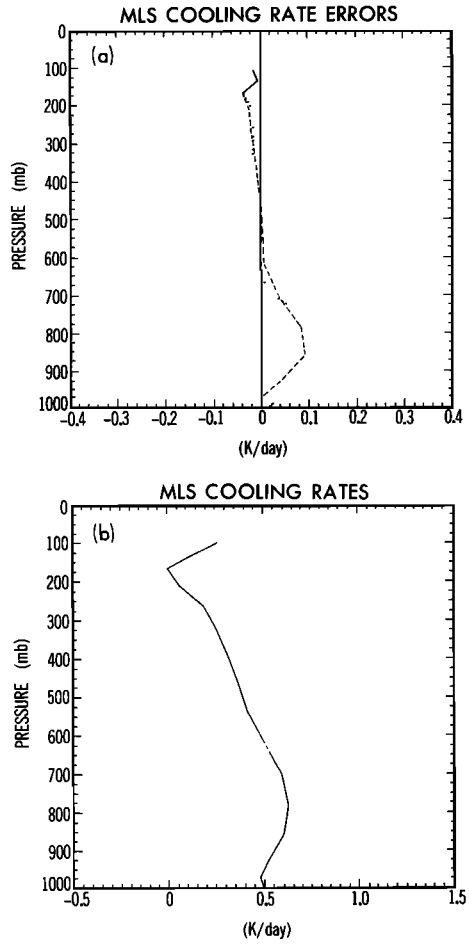

Fig. 23. (*a*) Cooling rate errors for the MLS profile in the 560–800 cm^{-1} range. Absorbers are CO_2 and H_2O (lines plus continuum). The dotted line is the one-band (Q_{app}) error, and the dashed line the error of the SEA88 calculation. The LBL cooling rates are given in Figure 23*b*. (*b*) LBL cooling rates for the MLS profile in the 560–800 cm^{-1} range. Absorbers are CO_2 and H_2O (lines plus continuum). Middle atmosphere results are not shown, since the vertical resolution used for these calculations is 20 mbar.

transmissivities. The pressure at which these Voigt effects become important is different for each absorber (since the Doppler width is proportional to wave number); in general, these Voigt effects become significant above about 10 mbar. Third, these narrowed line widths at low pressures allow the radiative computations to neglect the effect of overlap, and to calculate the effect of each absorber separately. Paradoxically, this effect introduces an additional complication in middle atmosphere computations; it becomes necessary to consider the contributions of a number of minor CO_2 and O_3 bands to middle atmosphere cooling rates, particularly near the stratopause. By contrast, the tropospheric radiative effects of these bands are obscured by overlap with H_2O, or with the major CO_2 or O_3 bands.

To determine how fully to parameterize these effects in the radiative algorithm, we may exploit the fact that the thermal structure of the middle atmosphere, unlike the troposphere, is largely under radiative control. It may be shown that an error in computation of radiative cooling rates at pressure p induces an error in the equilibrated temperature profile at that pressure according to the following approximate formulation:

$$\Delta T(p) \approx \tau_{rad} \Delta Q(p) \tag{26}$$

In this relation τ_{rad} is the radiative damping time at pressure p. This quantity has been obtained in a number of ways [e.g., *Fels*, 1982; *Kiehl and Solomon*, 1985]. Typical values for τ_{rad} are ~60 days at 50 mbar and ~5 days at 1 mbar. An error of 0.1 K/d thus results in an error of ~6 K at 50 mbar and of ~0.5 K at 1 mbar. We conclude that the radiative formulation must be very careful in evaluating effects in the lower stratosphere, but that significant errors (~0.2 K/d) are allowable at levels around and above the stratopause (1 mbar).

The above considerations lead us to a radiative algorithm which incorporates a number of modifications to the tropospheric methods described in section 4. The most important difference is the inclusion of ozone cooling by the 9.6-μm band. In addition, a simple parameterization of Voigt effects has been incorporated in the H_2O and O_3 calculations. The formulation allows for inclusion of some of the minor CO_2 and O_3 bands, as required for accuracy in calculations at various altitudes. A full discussion of these parameterizations is found below.

As in the tropospheric discussion, we validate the middle atmosphere radiative algorithm by comparison with benchmark LBL results. As noted in section 3 (Figures 2*b*-6*b*), middle atmosphere cooling rates for the five standard ICRCCM cases obtained by the SEA88 algorithm are generally in excellent agreement with the LBL results. Nonetheless, a number of differences are evident; inspection of these figures and of Figure 7*b* reveals three regions in which significant errors are made by the parameterized algorithms: above the 0.1-mbar level, at the stratopause level (around 1 mbar), and (most noticeably in the tropical calculation) in the lower stratosphere, around 50 mbar. For the purposes of this paper, the large errors evident at pressures lower then 0.1 mbar are of little concern, for at these altitudes a number of the assumptions made in the radiative calculations lose validity. In particular, the atmosphere deviates from the state of local thermodynamic equilibrium (LTE) beginning around 70 km, or 0.05 mbar; these non-LTE effects are not considered in this paper.

Cooling rate errors in the remaining altitude regions may be attributed to the approximations used by SEA88 in accounting for the middle atmosphere radiative effects discussed above. In the subsections below we discuss the treatment of the lower stratosphere in SEA88, with particular emphasis on the 9.6 μm ozone band computation, the sources of error in SEA88 at the stratopause region, and the effect of including Voigt effects in the H_2O and O_3 computations.

Lower Stratosphere Results and Issues

As noted above, the lower stratosphere is the region of the atmosphere where radiative formulations require the greatest accuracy. To investigate in greater detail the radiative processes responsible for cooling rates in this region, we have obtained cooling rates for the MLS profile separately for water vapor (lines plus continuum), CO_2 and O_3, using both the LBL method and the SEA88 algorithm. Figure 24*a* gives the LBL cooling rates for H_2O in the middle atmosphere, with errors due to the SEA88 formulation shown in

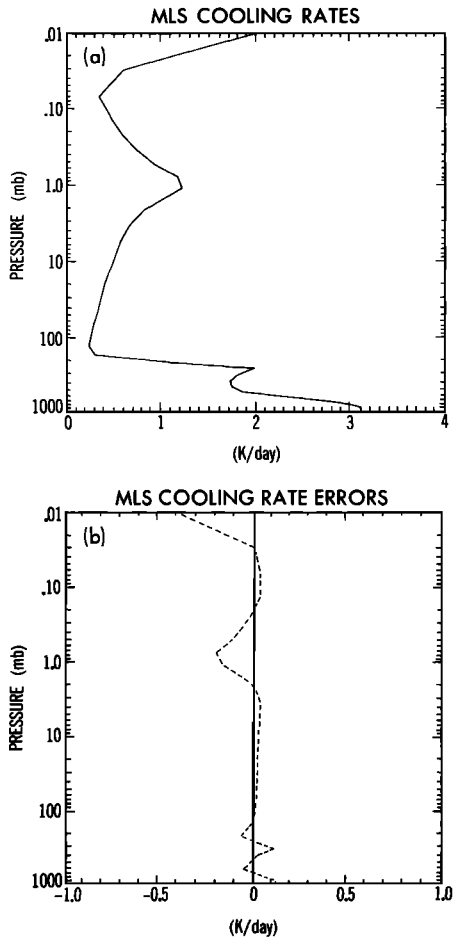

Fig. 24. (*a*) Cooling rates for the MLS profile in the middle atmosphere. The absorber is H_2O (lines plus continuum). The solid line is the LBL result for the 0–2200 cm^{-1} frequency range, with degraded vertical resolution employed. (*b*) Cooling rate errors for the MLS profile in the middle atmosphere. The absorber is H_2O (lines plus continuum). The dashed line gives the difference between the SEA88 computation and the LBL result shown in Figure 24*a*.

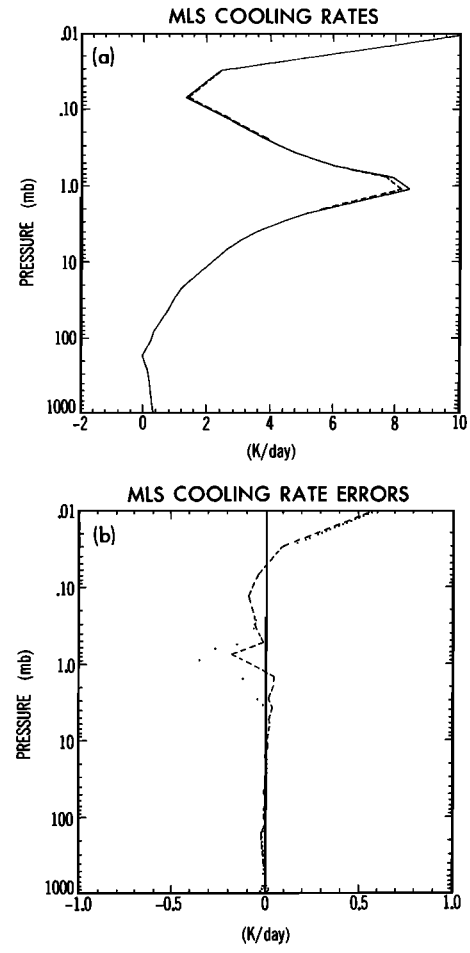

Fig. 25. (*a*) Cooling rates for the MLS profile in the middle atmosphere. The absorber is CO_2. The solid line gives LBL results for the 0–3000 cm^{-1} frequency range, and the dashed line the LBL results over the 490–850 cm^{-1} frequency range. Both calculations use the degraded vertical resolution. (*b*) Cooling rate errors for the MLS profile in the middle atmosphere. The absorber is CO_2. The dotted line gives the difference between the SEA88 computation and the LBL result for the 0–3000 cm^{-1} frequency range, and the dashed line gives the difference between the SEA88 computation and the LBL result for the 15-μm band (490–850 cm^{-1}).

Figure 24*b*. Figure 25*a* shows LBL cooling rates for CO_2; shown separately are cooling rates due only to the 15-μm band and due to the entire infrared spectrum. Figure 25*b* displays errors of the SEA88 method; since the SEA88 calculation includes only the 15-μm band, we have compared the results with the LBL 15-μm band cooling rates, as well as with the total infrared cooling rate. Figures 26*a* and 26*b* give corresponding results and errors for ozone; here results for the 9.6-μm band are displayed separately.

We supplement these results with Table 4, a detailed breakdown of LBL and SEA88 cooling rates at 47.9 mbar, a pressure representative of the lower stratosphere. The LBL results indicate that H_2O, CO_2, and O_3 each contribute importantly to cooling rates at this pressure, with the ozone giving a heating of ~0.40 K/d. The SEA88 results are in excellent agreement for all three gases. For H_2O and CO_2, these tabulations, as well as Figures 24*b* and 25*b*, indicate that the operational model successfully includes the contributions of all significant absorption features.

The situation regarding O_3 is far more complex. In the first place, ozone contributes a heating at this pressure, rather than a cooling. The difference arises from the sharp increase of climatological O_3 mixing ratio from the surface to ~50 mbar. As a result, the primary radiative process is the absorption of photons originating at the high-temperature regions nearer the surface by ozone molecules at low temperatures, resulting in radiative heating. In the 9.6-μm band (990–1070 cm^{-1}), the heating is enhanced by the lack of water vapor absorption in these frequencies. It is important to note, however, that a substantial proportion of the ozone heating in the LBL results arises outside of the 9.6-μm band; in fact, this band contributes only ~0.24 K/d to the O_3 heating. By contrast, the ozone heating in the operational model is entirely due to the 9.6-μm band. Thus the apparent agreement between SEA88 and LBL results is illusory; indeed, Figure 26*b* indicates that the SEA88 calculations overestimate heating in the 9.6-μm band by ~0.1 K/d throughout the lower stratosphere. This difference accounts for most of the error of ~0.09 K/d in the SEA88 calculation of overall cooling rates given in Table 4, as well as the errors of similar magnitude displayed in Figure 7*b*.

The 14.1-μm band of ozone, which contributes ~0.10 K/d

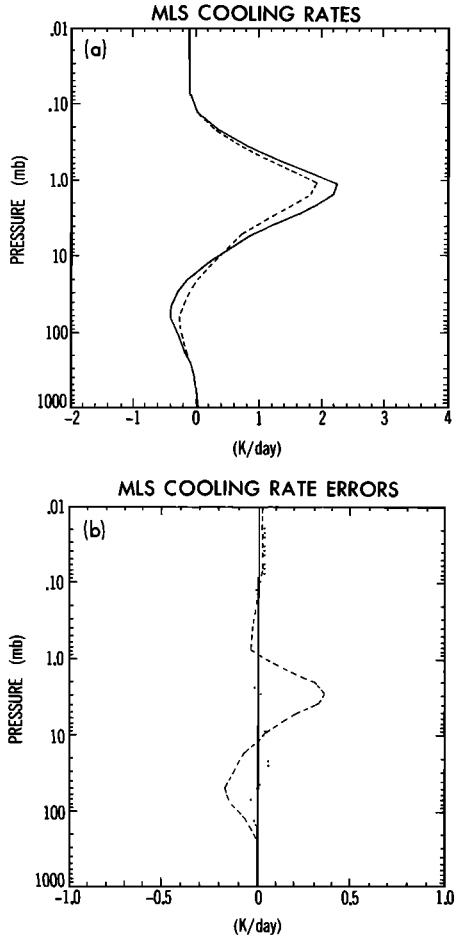

Fig. 26. (*a*) Cooling rates for the MLS profile in the middle atmosphere. The absorber is O_3. The solid line gives LBL results for the 0–3000 cm^{-1} frequency range, and the dashed line the LBL results over the 990–1070 cm^{-1} frequency range. Both calculations use the degraded vertical resolution. (*b*) Cooling rate errors for the MLS profile in the middle atmosphere. The absorber is O_3. The dotted line gives the difference between the SEA88 computation and the LBL result for the 0–3000 cm^{-1} frequency range, and the dashed line gives the difference between the SEA88 computation and the LBL result for the 9.6-μm band (990–1070 cm^{-1}).

to the O_3 heating in the LBL results, is entirely neglected in the operational model formulation. It is possible to justify this omission by noting that overlap with CO_2 largely eliminates any contribution of the 14.1-μm O_3 band to overall cooling rates in the lower stratosphere. For example, Table 4 indicates that elimination of the heating due to the 14.1-μm ozone band in the LBL calculations would greatly reduce the magnitude of the overlap term at this pressure; comparison of Figures 26*b* (indicating the magnitude of the heating due to the 14.1-μm band) and Figure 27, which displays the overlap effect, suggests that overlap between CO_2 and O_3 eliminates radiative effects of the 14.1-μm band at pressures greater than ~30 mbar.

In view of the errors in the 9.6-μm cooling rates shown in Figure 26*b*, it is necessary to justify the SEA88 ozone parameterization. In general, the computation of ozone cooling is a very complicated matter. A major factor in this complexity is that the use of pressure-scaled ozone amounts and mean pressures computed with the Curtis-Godson method appears to cause significant errors in ozone cooling rates [*Rodgers*, 1968]. Also, one-band Malkmus random models for ozone [*Malkmus*, 1967] are of questionable accuracy. It is especially unfortunate that the largest percentage errors in the pressure scaling occur at the very altitudes for which the radiative computations require the greatest accuracy. Moreover, it is impossible to use a CTS correction to handle this complication, since that correction is inapplicable when the dominate contribution to radiative cooling rates is heating from the ground. A number of investigators [*Rodgers*, 1968; *Goody*, 1964; *Kuriyan et al.*, 1977] have introduced improvements to the pressure scaling, or have employed multi-band Malkmus random models to obtain improved values for ozone cooling rates. Unfortunately, these changes are very costly in computer time. In the SEA88 formulation, we have therefore retained the one-band Malkmus random model formulation as a method for ozone computation. The band model parameters are obtained using the 1982 AFGL catalog. We intend to discuss improvements to these methods in a future paper.

Results and Issues at the Stratopause

Cooling rates for the MLS profile near the stratopause are displayed in Figure 3*b* (for the three-gas case) and in Figures 24*a*–26*b* (for LBL cooling rates and SEA88 cooling rate errors of the individual gaseous absorbers). As in the lower stratosphere, H_2O, CO_2 and O_3 all contribute significantly to cooling at these altitudes. Table 5 is a detailed breakdown of LBL and SEA88 cooling rates for the MLS profile at the 1.08-mbar level, a level representative of the stratopause region. The total LBL cooling rate for the three gases is ~11.9 K/d, with ~1.2 K/d owing to H_2O, ~8.4 K/d to CO_2, and ~2.2 K/d to O_3. At this level, the sum of the individual contributions of the three gases is almost identical to the cooling rated computed with all three gases taken together at once, indicating that overlap is unimportant. A significant fraction of the cooling due to CO_2 and O_3 occurs outside the 15-μm CO_2 and 9.6-μm O_3 bands; at this height, cooling due to the 14.1-μm O_3 band amounts to 0.22 K/d, while cooling from the 4.3-μm and 10-μm bands of CO_2 (mostly the former) totals 0.23 K/d.

Table 5 and Figure 7*b* both indicate that the SEA88 cooling rate at this altitude underestimates the LBL cooling by ~0.8 K/d. The LBL results indicate that the neglect of the 4.3-μm band of CO_2 and the 14.1-μm band of O_3 in SEA88 accounts for ~0.45 K/d. The remaining difference of ~0.35 K/d is mainly attributable to the techniques used by SEA88 to incorporate Voigt effects in computing H_2O and O_3 cooling rates. These techniques will be discussed in the next subsection.

As noted above, errors in radiative cooling rates at altitudes near the stratopause result in much smaller changes in general circulation model temperature profiles than result from errors made in the lower stratosphere. In the present SEA88 calculations, we have excluded the contributions of the minor bands of O_3 and CO_2. To include these mechanisms in the future (at some cost in computation time) we may compute cooling rates due to these bands in the random CTS calculation. As indicated in Figure 1, most cooling at these altitudes is indeed due to escape of photons to space; furthermore, pressure scaling is likely to be more accurate in this region than in the lower stratosphere, as CO_2 and O_3 mixing ratios are constant with altitude, or decrease.

TABLE 4. Cooling Rates at the 47.9-mbar Pressure Level (in K/d) Obtained Using the SEA88 and LBL Methods for $Q(H_2O)$, $Q(CO_2)$, $Q(O_3)$, and for All Gases $Q(H_2O + CO_2 + O_3)$

			LBL Cooling Rates by Bands				
			CO_2 Bands			O_3 Bands	
	Overall Cooling Rates		15 μm	10 μm	4.3 μm	9.6 μm	14.1 μm
Absorber	SEA88	LBL	490–850	900–1090	2270–2380	990–1070	630–800
H_2O	0.346	0.326					
CO_2	0.655	0.661	0.665	−0.002	0.000		
O_3	−0.408	−0.400				−0.235	−0.100
All gases	0.610	0.701					
Overlap	0.017	0.114					

Overall LBL cooling rates are given for the 0–3000 cm^{-1} frequency range. In addition, LBL cooling rates for CO_2 and O_3 are broken down by major absorption bands, with the frequency ranges given in cm^{-1}. Overlap is the difference between the cooling rate for all gases and the cooling rate obtained by summing the cooling rates due individually to H_2O, CO_2, and O_3. The LBL cooling rates are degraded from high vertical resolution calculations using procedures given in the appendix.

Voigt Effects in Middle Atmosphere Radiative Calculations

An important problem in middle atmospheric radiative calculations is determining a method for inclusion of the additional cooling resulting from the fact that the spectral line width at low pressures is wider than that expected by a Lorentz profile. Except for CO_2, it is entirely impractical to use the actual (Voigt) profile, and thus approximate treatments must be sought.

One of the simplest means for capturing the effect of the Voigt profile has been suggested by *Fels* [1979]. In that paper an analytic line shape profile was introduced and applied to ozone computations. Even this method is too time-consuming for use in general circulation models. However, a second crude approximation is also suggested in the paper; this consists of adding a constant to the pressure (in atmospheres) used in the line width computation:

$$p/p_0 \rightarrow p/p_0 + c \tag{27}$$

In (27), c is a number which may depend on the gaseous absorber, and p_0 is the standard surface pressure. We have used this approximation in SEA88 for the O_3 and H_2O radiative computations. The values chosen for c are 0.004 for ozone, and 0.0003 for H_2O. The smaller value of c in the H_2O computation is consistent with the observation (cf. Figure 11) that most H_2O cooling in the middle atmosphere is at wavenumbers far smaller than those of the 9.6-μm ozone band. Doppler widths for H_2O lines providing significant cooling are therefore much smaller than those of the ozone lines. The great virtue of the above technique is that it is almost cost-free, in terms of computation time.

Figure 28 displays LBL and operational model H_2O calculations made with and without the Voigt parameterization. The use of the Voigt correction greatly improves the H_2O results at 0.1 mbar; at the stratopause, the discrepancies are somewhat reduced, to about 0.2 K/d. Figure 29 shows the corresponding LBL and operational model results for ozone, showing the effect of the Voigt correction. At the stratopause, the Voigt ozone formulation is seen to underestimate ozone cooling by about 0.2 K/d. The necessity of inclusion of ozone Voigt effects is clear, as the difference in cooling rates is as large as 0.7 K/d near the stratopause.

6. Computational Considerations

At present, the SEA88 radiation algorithm computes cooling rates and fluxes for a 40-level sounding in about 0.003 s/grid point on the GFDL Cyber 205 computer. This timing is about 10% faster than that for the GFDL operational radiation code based on SEA75. The improvement in speed is largely due to the reduction in the number of frequency bands in the random CTS computation, owing to the use of the combined narrow band approximation.

Since the model timing depends on the number of pressure levels, as well as the computer employed, it is more useful to discuss the breakdown of the model computation time in terms of the fraction of total time spent in each of the major code sections. The fundamental relation of the SEA method

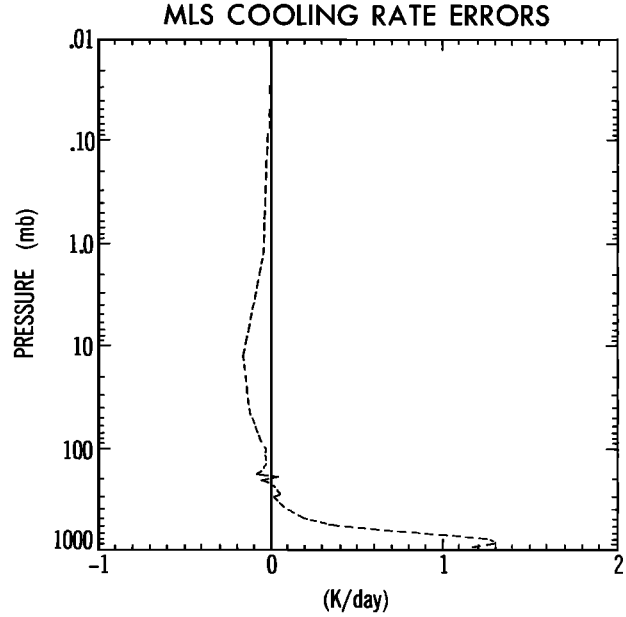

Fig. 27. Effect of overlap on LBL cooling rates. The dashed line gives the difference between LBL computations of individual cooling rates and LBL computation of cooling rates for all absorbers, i.e., $(Q(H_2O) + Q(CO_2) + Q(O_3)) - (Q(H_2O + CO_2 + O_3))$. The MLS profile is used over the 0–3000 cm^{-1} frequency range. Resolution effects are responsible for the oscillations near 100 mbar.

TABLE 5. Cooling Rates at the 1.08-mbar Pressure Level (in K/d) Obtained Using the SEA88 and LBL Methods for $Q(H_2O)$, $Q(CO_2)$, $Q(O_3)$, and for All Gases $Q(H_2O + CO_2 + O_3)$

			LBL Cooling Rates by Bands				
			CO_2 Bands			O_3 Bands	
	Overall Cooling Rates		15 μm	10 μm	4.3 μm	9.6 μm	14.1 μm
Absorber	SEA88	LBL	490–850	900–1090	2270–2380	990–1070	630–800
H_2O	1.05	1.21					
CO_2	8.07	8.40	8.14	0.02	0.21		
O_3	1.96	2.22				1.90	0.22
All gases	11.09	11.88					
Overlap	0.01	0.05					

Overall LBL cooling rates are given for the 0–3000 cm^{-1} frequency range. In addition, LBL cooling rates for CO_2 and O_2 are broken down by major absorption bands, with the frequency ranges given in cm^{-1}. Overlap is the difference between the cooling rate for all gases and the cooling rate obtained by summing the cooling rates due individually to H_2O, CO_2, and O_3. The LBL cooling rates are degraded from high vertical resolution calculations using procedures given in the appendix.

is (9), which divides the cooling rate into the approximate, approximate CTS and random CTS cooling rates. If we determine the time spent computing each of these terms, we find that the GFDL Cyber 205 computer spends ~72% of the total time in obtaining Q^{app}, ~3% in computing Q_{CTS}^{app}, and ~25% in determining Q_{CTS}^{random}. (These percentages have been obtained for a cloud-free case using 40 model levels; minor changes are expected if fewer pressure levels are used). The CTS calculations thus require about 30 percent of the model calculation time. This additional computational burden is justifiable for most purposes, in light of the large improvements to tropospheric cooling rates obtained using the CTS correction (cf. Figure 7*a*).

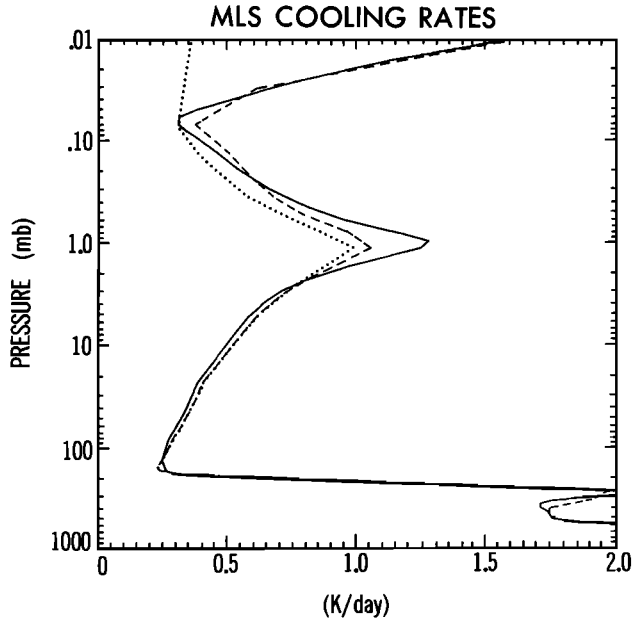

Fig. 28. Cooling rates for the MLS profile in the middle atmosphere for H_2O (lines plus continuum) showing the effect of the Voigt correction. The solid line gives the LBL result, the dotted line the SEA88 result without a Voigt correction, and the dashed line the SEA88 result with the adopted Voigt correction.

7. SUMMARY AND CAUTION

The fast parameterization for longwave cooling rate calculations presented in this paper is one of a new generation of operational radiation models. These differ from their predecessors in that they have been carefully calibrated with respect to benchmark line-by-line calculations. Ours is not the only such code; several others of comparable speed and accuracy are currently under development. As the use of ICRCCM benchmarks as a calibration standard becomes more widespread, it is reasonable to expect that various well-constructed parameterizations will give results which cluster tightly around the benchmark values.

A major remaining issue is the accuracy of the LBL calculations. The most important problems here are the validity of the spectral input data and the uncertainties in such matters as the line shape or the temperature dependence of line widths. Line strengths, widths and positions

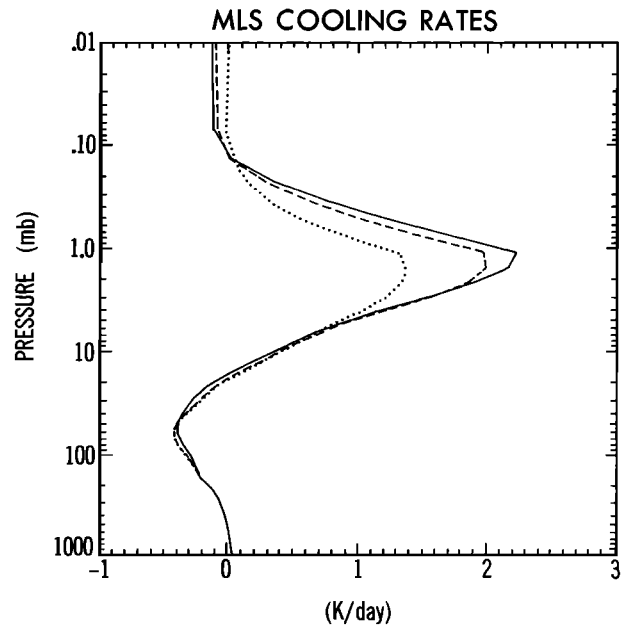

Fig. 29. Same as Figure 28, but for O_3.

are obtained by means of laboratory measurements over homogeneous paths. Unfortunately, the parameter range over which the spectral data are taken is very often far from that required for the calculation of terrestrial atmospheric fluxes. Further, these measurements indicate that line shapes and temperature dependences differ significantly from established theoretical constructs such as the Lorentz line shape. This forces us to adopt a number of semitheoretical methods to permit absorptivities computed by LBL methods to agree with laboratory measurements.

While there is currently little reason to suspect that there are serious difficulties with the LBL methods, a definitive answer must await careful observation of fluxes in the actual atmosphere. An interesting step in this direction is the comparison of satellite observed fluxes at the top of the atmosphere with those calculated from well-calibrated theoretical models. Such studies have been carried out by *Ramanathan and Downey* [1986*b*] using Earth Radiation Budget Experiment (ERBE) data. By choosing stringently selected clear-sky cases, they find excellent agreement between theory and observation. This increases confidence in the correctness of the theoretical model and thus, by extension, in the results from a carefully calibrated parameterized algorithm such as the one described in this paper.

APPENDIX: LBL AND MODEL PROFILES

Temperature, water vapor, and ozone profiles in this paper are taken from the five standard profiles given by *McClatchey et al.* [1971]. These profiles specify atmospheric quantities at 1-km intervals from the surface to 25 km, at 5-km intervals from 25 to 50 km, and at 70 and 100 km. In the present calculations, we have employed very different pressure level structures; this appendix is concerned with the methods used to interpolate the AFGL profiles to our pressure specifications.

Four pressure structures are used in the calculations for this paper. (In the following, the pressures at which temperatures and mixing ratios are given for radiative calculations are called data pressure levels; pressures at which radiative fluxes are computed are denoted as flux pressure levels.) Three specifications of flux pressure levels are used for the LBL computations. For water vapor calculations, 52 flux levels are used, with the levels spaced from 0 to 1000 mbar at 20-mbar intervals, and an additional flux level located at the surface. Ozone and CO_2 computations employ 108 flux levels. In this case, flux levels are spaced evenly in the logarithm of pressure, with 15 levels per decade of pressure (between 10^{-3} and 10^{2} mbar) and 30 levels between 100 and 1000 mbar. Flux levels are also located at 0 mbar and at the surface. This level structure is identical to that described in SF85 for LBL CO_2 calculations. LBL computations involving all three gases employ a level structure with 123 flux levels, with levels below 100 mbar using the CO_2 structure, and levels above 100 mbar using the H_2O structure. In all three cases, the data pressure level is defined as the average of adjacent flux pressure levels. These choices are designed to produce the greatest resolution at altitudes where the contribution of the absorber is most significant.

Calculations made with the new operational model use a 40-level structure normally employed at GFDL for the 40-level stratospheric model (see *Fels et al.* [1980] for details on this level structure). In this case, flux pressure levels are defined as the average of adjacent data pressure levels.

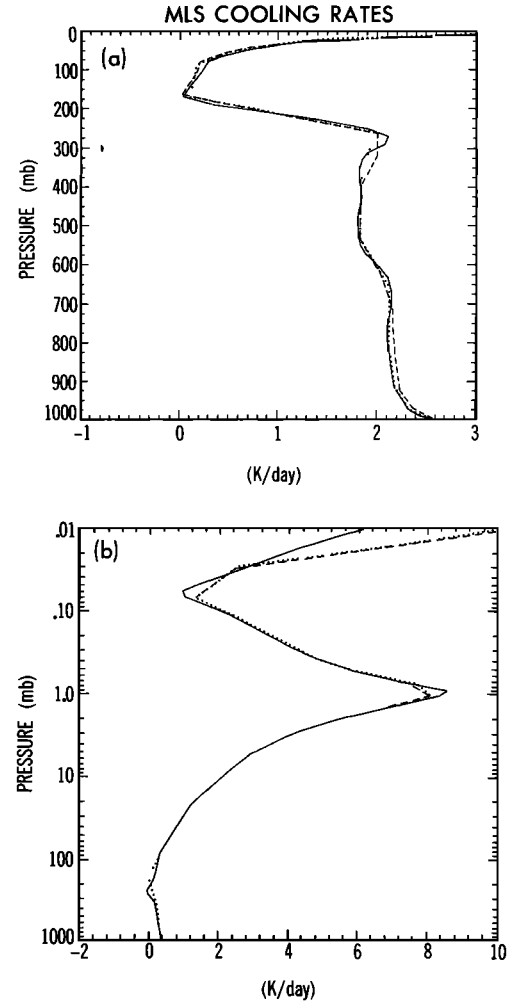

Fig. 30. (*a*) Tropospheric cooling rates for the MLS profile, with absorption from all gases included. The solid line gives LBL results (as in Figure 2*a*), the dotted line gives LBL results with resolution degraded to the pressure levels used in SEA88 calculations, and dashed line gives the SEA88 results. (*b*) Cooling rates for the MLS profile in the middle atmosphere for CO_2. The solid line gives the LBL result over the 490–850 cm^{-1} frequency range. The dotted line is the same result, but with the pressure level resolution degraded to that of the operational model. The dashed line is the cooling rate obtained by SEA88 for CO_2 in the 560–800 cm^{-1} range.

As noted in sections 4 and 5, the differing resolution of the LBL and operational models can introduce artificial errors in comparing LBL and operational model results. To evaluate the magnitude of these errors, we have computed LBL cooling rates on the operational model level structure. The procedure used involves a linear interpolation of the net radiative fluxes computed at LBL flux pressure levels onto the flux pressure levels of the operational model. Cooling rates are then obtained from these interpolated fluxes, using (1). As Figures 30*a* and 30*b* indicate, "degraded" LBL cooling rates obtained on the operational model pressure structure may differ substantially from the "exact" LBL results, especially below 1 mbar and in the upper troposphere.

The temperature profiles used for the LBL and the operational model profiles are interpolated from the AFGL

profiles using a technique given by *Fels* [1986]. This method has been adopted for the ICRCCM study.

Water vapor mass mixing ratios are obtained by evaluation of analytic fits to each of the AFGL profiles at desired pressure levels. These fits have been suggested by Luther for use in the ICRCCM study. A constant mixing ratio (3.25 ppmm for the tropical profile, and 4.0 ppmm for the other profiles) is used for altitudes above the troposphere.

Ozone mass mixing ratios are obtained from the AFGL values by the following procedure: (1) the tabulated ozone values (given in g/m^3) are linearly interpolated to desired pressures, and (2) the mass mixing ratio is computed using the ideal gas law. This procedure requires knowledge of the temperature at the desired pressure level. The use of a linear interpolation results in inaccuracies in the ozone amounts above 50 km, and should not be used in future work, but the errors do not affect conclusions in this paper. It is important to note that tabulated values of air density given by *McClatchey et al.* [1971] for the MLS sounding are erroneous between 30 and 70 km. Therefore the more direct procedure of obtaining the ozone mixing ratio by dividing the tabulated ozone values by this density should not be used.

Acknowledgments. S. Manabe and V. Ramaswamy provided valuable comments. The suggestions of two anonymous reviewers have been very helpful. The GFDL drafting group skillfully prepared the figures.

REFERENCES

Chedin, A., N. Husson, N. A. Scott, I. Cohen-Hallaleh, and A. Berroir, The GEISA data bank, 1984 version, *Internal Note 127*, Lab. de Meteorol. Dyn. du Cent. Natl. de la Rech. Sci., Ecole Polytech., Palaiseau, France, 1985.

Clough, S. A., F. X. Kneizys, R. Davies, R. Gamache, and R. Tipping, Theoretical line shape for H_2O vapor: Application to the continuum, in *Atmospheric Water Vapor*, edited by A. Deepak, T. D. Wilkerson, and L. H. Ruhnke, pp. 25–41, Academic, San Diego, Calif., 1980.

Crisp, D., S. B. Fels, and M. D. Schwarzkopf, Approximate methods for finding CO_2 15-μm band transmission in planetary atmospheres, *J. Geophys. Res.*, *91*, 11,851–11,866, 1986.

Drayson, S. R., Atmospheric transmission in the CO_2 bands between 12μ and 18μ, *Appl. Opt.*, *5*, 385–391, 1973.

Fels, S. B., Simple strategies for inclusion of Voigt effects in infrared cooling calculations, *App. Opt.*, *18*, 2634–2637, 1979.

Fels, S. B., A parameterization of scale-dependent radiative damping in the middle atmosphere, *J. Atmos. Sci.*, *39*, 1141–1152, 1982.

Fels, S. B., Analytic representations of standard atmosphere temperature profiles, *J. Atmos. Sci.*, *43*, 219–221, 1986.

Fels, S. B., and M. D. Schwarzkopf, The simplified exchange approximation: A new method for radiative transfer calculations, *J. Atmos. Sci.*, *32*, 1475–1488, 1975.

Fels, S. B., and M. D. Schwarzkopf, An efficient, accurate algorithm for calculating CO_2 15μ band cooling rates, *J. Geophys. Res.*, *86*, 1205–1232, 1981.

Fels, S. B., J. D. Mahlman, M. D. Schwarzkopf, and R. W. Sinclair, Stratospheric sensitivity to perturbations in ozone and carbon dioxide: Radiative and dynamical response, *J. Atmos. Sci.*, *37*, 2266–2297, 1980.

Fels, S. B., J. T. Kiehl, A. A. Lacis, and M. D. Schwarzkopf, Infrared cooling rate calculations in operational general circulation models: Comparisons with benchmark computations, *J. Geophys. Res.*, this issue.

Goody, R. M., The transmission of radiation through an inhomogeneous atmosphere, *J. Atmos. Sci.*, *21*, 575–581, 1964.

Grant, W. B., A critical review of measurements of water vapor absorption in the 840 to 1100 cm^{-1} spectral region, *JPL Publ.*, *87-34*, 1987.

Kiehl, J. T., and S. Solomon, On the radiative balance of the stratosphere, *J. Atmos. Sci.*, *43*, 1525–1534, 1986.

Kuriyan, J. G., Z. Shippony, and S. K. Mitra, Transmission functions for infrared radiative transfer in an inhomogeneous atmosphere, *Q. J. R. Meteorol. Soc.*, *103*, 511–517, 1977.

Leovy, C. B., Infrared radiative exchange in the middle atmosphere in the 15 micron band of carbon dioxide, in *Dynamics of the Middle Atmosphere*, edited by J. R. Holton and T. Matsuno, pp. 355–366, D. Reidel, Hingham, Mass., 1984.

Luther, F. M., R. G. Ellingson, Y. Fouquart, S. B. Fels, N. Scott, and W. J. Wiscombe, Intercomparison of radiation codes in climate models (ICRCCM): Longwave clear-sky results—A workshop summary, *Bull. Am. Meteorol. Soc.*, *69*, 40–48, 1988.

Malkmus, W., Random Lorentz band model with exponential-tailed S^{-1} line intensity distribution function, *J. Opt. Soc. Am.*, *57*, 323–329, 1967.

McClatchey, R. A., W. Fenn, J. E. A. Selby, F. E. Volz, and J. S. Garing, Optical properties of the atmosphere, *Rep. AFCRL-71-0279*, Air Force Cambridge Res. Lab., Hanscom Air Force Base, Bedford, Mass., 1971.

McClatchey, R. A., W. S. Benedict, S. A. Clough, D. E. Burch, R. F. Calfee, K. Fox, L. S. Rothman, and J. S. Garing, AFCRL atmospheric absorption line parameters compilation, *Rep. AFCRL-TR-73-0096*, 83 pp., Air Force Cambridge Res. Lab., Hanscom Air Force Base, Bedford, Mass., 1973.

Ramanathan, V., and P. Downey, A nonisothermal emissivity and absorptivity formulation for water vapor, *J. Geophys. Res.*, *91*, 8649–8666, 1986*a*.

Ramanathan, V., and P. Downey, An approach to verifying clear-sky radiation models with ERBS scanner measurements, in *Extended Abstracts of the Sixth Conference on Atmospheric Radiation*, pp. J28–J31, American Meteorological Society, Boston, Mass., 1986*b*.

Ridgway, W. L., Harshvardhan, and A. Arking, Computation of atmospheric infrared cooling rates by exact and approximate methods, *J. Geophys. Res.*, this issue.

Roberts, E., J. E. A. Selby, and I. M. Biberman, Infrared continuum absorption by atmospheric water vapor in the 8–12 μm window, *Appl. Opt.*, *15*, 2085–2090, 1976.

Rodgers, C. D., Some extensions and applications of the new random model for molecular band transmission. *Q. J. R. Meteorol. Soc.*, *94*, 99–102, 1968.

Rodgers, C. D., and C. D. Walshaw, The computation of infrared cooling rate in planetary atmospheres, *Q. J. R. Meteorol. Soc.*, *92*, 67–92, 1966.

Rothman, L. S., Atmospheric absorption line parameters compilation: 1980 version, *Appl. Opt.*, *20*, 791–795, 1981.

Rothman, L. S., R. R. Gamache, A. Barbe, A. Goldman, J. R. Gillis, L. R. Brown, R. A. Toth, J. M. Flaud, and C. Camy-peyret, AFGL atmospheric absorption line parameters compilation: 1982 edition, *Appl. Opt.*, *22*, 2247–2256, 1983.

Rothman, L. S., et al., The HITRAN data base: 1986 edition, *Appl. Opt.*, *26*, 4058–4097, 1987.

Schwarzkopf, M. D., Aspects of longwave fluxes and cooling rates computed with a line-by-line model, in *Extended Abstracts of the Sixth Conference on Atmospheric Radiation*, pp. 183–184, American Meteorological Society, Boston, Mass., 1986.

Schwarzkopf, M. D., and S. B. Fels, Improvements to the algorithm for computing CO_2 transmissivities and cooling rates, *J. Geophys. Res.*, *90*, 10,541–10,550, 1985.

Suck, S. H., J. L. Kassner, Jr., and Y. Yamaguchi, Water cluster interpretation of IR absorption spectra in the 8-14 μm wavelength region, *Appl. Opt.*, *18*, 2609–2617, 1979.

World Meteorological Organization, World Climate Programme, The Intercomparison of Radiation Codes in Climate Models (ICRCCM)—Longwave Clear-Sky Calculations, *Rep. WCP-93*, prepared by F. M. Luther, Geneva, 1984.

M. D. Schwarzkopf, NOAA Geophysical Fluid Dynamics Laboratory, P. O. Box 308, Princeton University, Princeton, NJ 08542.

(Received November 17, 1988;
revised March 30, 1989;
accepted July 10, 1989.)